AFRL-RX-WP-TM-2010-4182

COLLABORATIVE RESEARCH AND DEVELOPMENT (CR&D)

Delivery Order 0031: Basic Research and Development of Ti-B Alloys

Seshacharyulu Tamirisakandala

Ohio University

SEPTEMBER 2006
Final Report

AIR FORCE RESEARCH LABORATORY
MATERIALS AND MANUFACTURING DIRECTORATE
WRIGHT-PATTERSON AIR FORCE BASE, OH 45433-7750
AIR FORCE MATERIEL COMMAND
UNITED STATES AIR FORCE

NOTICE AND SIGNATURE PAGE

AFRL-RX-WP-TM-2010-4182 HAS BEEN REVIEWED AND IS APPROVED FOR PUBLICATION IN ACCORDANCE WITH THE ASSIGNED DISTRIBUTION STATEMENT.

*//Signature//

MARK GROFF
Program Manager
Business Operations Branch
Materials & Manufacturing Directorate

//Signature//

KENNETH A. FEESER
Branch Chief
Business Operations Branch
Materials & Manufacturing Directorate

*Disseminated copies will show "//Signature//" stamped or typed above the signature blocks.

REPORT DOCUMENTATION PAGE	*Form Approved OMB No. 0704-0188*

1. REPORT DATE *(DD-MM-YY)*	2. REPORT TYPE	3. DATES COVERED *(From - To)*
September 2006	Final	02 September 2004 – 05 September 2006

4. TITLE AND SUBTITLE
COLLABORATIVE RESEARCH AND DEVELOPMENT (CR&D)
Delivery Order 0031: Basic Research and Development of Ti-B Alloys

5a. CONTRACT NUMBER F33615-03-D-5801-0031
5b. GRANT NUMBER
5c. PROGRAM ELEMENT NUMBER 62102F

6. AUTHOR(S)
Seshacharyulu Tamirisakandala

5d. PROJECT NUMBER 4349
5e. TASK NUMBER L0
5f. WORK UNIT NUMBER 4349L0VT

7. PERFORMING ORGANIZATION NAME(S) AND ADDRESS(ES)

By:	For
Ohio University Athens, OH	Universal Technology Corporation 1270 North Fairfield Road Dayton, OH 45432-2600

8. PERFORMING ORGANIZATION REPORT NUMBER S-531-031

9. SPONSORING/MONITORING AGENCY NAME(S) AND ADDRESS(ES)
Air Force Research Laboratory
Materials and Manufacturing Directorate
Wright-Patterson Air Force Base, OH 45433-7750
Air Force Materiel Command
United States Air Force

10. SPONSORING/MONITORING AGENCY ACRONYM(S) AFRL/RXOB
11. SPONSORING/MONITORING AGENCY REPORT NUMBER(S) AFRL-RX-WP-TM-2010-4182

12. DISTRIBUTION/AVAILABILITY STATEMENT
Approved for public release; distribution unlimited.

13. SUPPLEMENTARY NOTES
PAO Case Number: 88ABW 2010-1228; Clearance Date: 17 Mar 2010. Research for this report ended in 2006. Report contains color.

14. ABSTRACT
This research in support of the Air Force Research Laboratory, Materials and Manufacturing Directorate was conducted at Wright-Patterson AFB, Ohio from 2 September 2004 through 5 September 2006. Studies on important Ti alloys modified with different boron levels were conducted to advance the technology of Ti-B alloys. Fundamental scientific understanding on effects of boron addition on the microstructural characteristics of titanium alloys was obtained. Influence of boron addition on the thermomechanical processing (TMP) response of Ti alloys was studied via well-thought and conducted experiments. Benefits offered by boron enhancement in terms of reduction or elimination of expensive TMP steps were explored and novel processing sequences were suggested to improve the affordability of titanium aerospace components. Efforts to scale-up from lab-scale to production-scale were initiated and key features to be measured and verified for technology transition were identified. Collaborative efforts with extramural teams working in related research areas were established to augment the RX in-house research effort. The research findings were presented at International conferences and published in peer-reviewed journals. These studies provided paths for successful design of novel titanium microstructures that possess useful property combinations for static as well as fracture-critical applications.

15. SUBJECT TERMS
titanium alloys, boron addition, microstructure, mechanical properties, processing, characterization

16. SECURITY CLASSIFICATION OF:			17. LIMITATION OF ABSTRACT:	18. NUMBER OF PAGES	19a. NAME OF RESPONSIBLE PERSON (Monitor)
a. REPORT	b. ABSTRACT	c. THIS PAGE			Mark Groff
Unclassified	Unclassified	Unclassified	SAR	60	19b. TELEPHONE NUMBER *(Include Area Code)* N/A

Standard Form 298 (Rev. 8-98)
Prescribed by ANSI Std. Z39-18

TO-31: Basic Research and Development of Ti-B Alloys

Executive Summary

This report is organized into the following 5 tasks and summary of each task is described in subsequent sections.

Task 1: Affordable and Advanced Titanium Alloys via Boron Addition

Task 2: Development of Affordable Beta Titanium Alloys

Task 3: Affordable Superplastic Forming of Titanium Alloys

Task 4: Three-Dimensional Characterization of Ti-B Alloy Microstructures

Task 5: In situ Deformation Studies on Ti-B Alloys

The following publications emanated from this research effort, which were published in peer-reviewed international journals. Complete descriptions of the results obtained in the above tasks are provided in these publications. Copies of the published articles are included in Attachment 1.

1. Grain Refinement of Titanium Alloys via Trace Boron Addition
   S. Tamirisakandala, R.B. Bhat, J.S. Tiley, and D.B. Miracle
   Scripta Materialia, 53 (2005), pp. 1421-1426.
2. Processing, Microstructure, and Properties of Beta Titanium Alloys Modified With Boron
   S. Tamirisakandala, R.B. Bhat, J.S. Tiley, and D.B. Miracle
   Journal of Materials Engineering and Performance, 14, 6 (2005), pp. 741-746.
3. Reconstruction of three-dimensional microstructures of TiB phase in a powder metallurgy titanium alloy using montage serial sectioning
   S. I. Lieberman, A.M. Gokhale, and S. Tamirisakandala
   Scripta Materialia, 55 (2006), pp. 63-68.
4. In situ scanning electron microscopy observations of tensile deformation in a boron-modified Ti–6Al–4V alloy
   C.J. Boehlert, C.J. Cowen, S. Tamirisakandala, D.J. McEldowney, and D.B. Miracle
   Scripta Materialia, 55 (2006) pp. 465–468.
5. Reconstruction of Three-Dimensional Microstructures of TiB Whiskers in Powder Processed Ti-6Al-4V-1B Alloys
   S. I. Lieberman, A.M. Gokhale, and S. Tamirisakandala
   Materials Characterization, In Press

One patent application titled "Method of Producing High Strength, High Stiffness and High Ductility Titanium Alloys" was filed with US Patents and Trademarks Office in June 2006. Copy of the patent application is included in Attachment 2.

Research work performed during the reporting period effort was presented at the several international conferences and the list of presentations is given below.

1. Affordable Ti-B Alloys for Aerospace Applications: Microstructure and Morphology Evolution
   Invited presentation at the *International Conference on Solidification Science and Processing*, 17-20 Nov 2004, Bangalore, India.
2. Affordable Titanium Alloys via Boron Additions
   Invited presentation at *The 3rd International Conference on Advanced Materials Processing*, Melbourne, Australia, 29 Nov-1 Dec 2004.
3. Processing, Microstructure, and Properties of Beta Ti Alloys Modified with Boron
   International symposium on *Beta Titanium Alloys of 00's*, TMS Annual Meeting, Feb 13-17, 2005, San Francisco, CA
4. Microstructural Evolution during Hot Working of Ti-B Alloys
   14^{th} Advanced Aerospace Materials and Processes Conference (AEROMAT), June 6-9, 2005, Orlando, FL.
5. Grain Refinement of Titanium Alloys via Trace Boron Addition
   Materials Science and Technology 2005, Sep 25-28, 2005, Pittsburgh, PA.
6. Microstructural Refinement of Titanium Alloys via Boron Addition
   Workshop on Titanium Alloys Modified with Boron
   Oct 11-13, 2005, Dayton, OH
7. An Overview of Titanium Alloys Modified with Boron
   Invited Presentation at the AEROMAT 2006, Seattle, May 2006
8. Development of Affordable and Advanced Titanium Alloys for Potential Aerospace Applications
   Keynote presentation at the Advances in Materials and Processing Technologies (AMPT), Las Vegas, July 30-Aug 3, 2006

2

Task1: Affordable and Advanced Titanium Alloys via Boron Additions

The objective of this task is to explore affordable processing methodologies to produce high structural efficiency Ti-B alloys with controlled microstructures.

Ti-B alloy castings with the following compositions were procured from a commercial casting company (Flowserve corporation, Dayton, OH): CP Ti with 0.02, 0.1, and 0.4B; Ti-6Al-4V with 0, 0.02, 0.05, 0.1, 0.4, and 1.0B; and Ti-6Al-2Sn-4Zr-2Mo-0.1Si with 0, 0.1, 0.5, and 1.0B. These castings were produced via induction skull melting (ISM) and cast into 2.8″ diameter × 20″ length ingots using graphite molds. All the castings were hot isostatically pressed at 900°C/100 MPa/2 h to seal any shrinkage porosity. The ingots were radiographically examined after HIP and found to be free from porosity. Chemical analysis and microstructural examination of the materials from top and bottom portions of the ingots revealed good chemical and microstructural homogeneity throughout the ingot. The boride phase formed in situ due to boron addition was confirmed to be TiB from X-ray diffraction. Detailed microstructural examination on all the Ti-B alloys was performed using optical and scanning electron microscopy. Digital image analysis was used to quantify the microstructural features. Tensile properties at room temperature as well as elevated temperatures up to 600°C were evaluated per ASTM E-8 standard. Key results of this task are summarized below.

- Conventional casting technique (ISM) could be successfully used to produce Ti-B alloys that are chemically and microstructurally homogeneous. Boron could be simply added as an additional alloying element and excellent control on the amount of boron was achieved. This demonstrates that affordable melt processing techniques could be used to produce Ti-B alloys.
- Minor additions of boron to Ti alloys produced dramatic (10X) reduction in the as-cast grain size (Fig. 1 and 2). In conventional Ti-6Al-4V, as-cast grain size of about 2 mm was refined to about 200 μm by adding a trace amount of boron in the range 0.05-0.1 wt.%. Traditionally, extensive thermo-mechanical processing involving ingot breakdown conducted via repetitive hot working in the beta phase field is essential to breakdown and refine the coarse as-cast microstructure. Ability to achieve fine grain size in the as-cast condition eliminates the ingot breakdown operation and enhances affordability of titanium components.
- Addition of minor amounts of boron to Ti alloys produces significant grain refinement without any deterioration in ductility (Fig. 2). Grain refinement in fact was found to enhance ductility of the as-cast material. For example, the ductility levels were maintained at 10% for 0.1% boron modified Ti-64.
- Grain refinement due to minor boron addition also enhances strength and the TiB that forms in situ was found to enhance the stiffness. Increase in strength and

stiffness by 5% were observed by adding 0.1% boron. Higher (1%) boron additions further increase the stiffness and strength up to 30% with reduction in ductility. The property data as a function of boron concentration would help in the design to optimize the boron level for the desired property combination.

- The strength enhancements due to boron additions were maintained at elevated temperatures also up to 550°C (Fig. 3). Higher elevated temperature strength via boron addition expands the maximum service temperature of the conventional Ti alloys, which provides additional affordability.
- Microstructural observations revealed the presence of TiB precipitates at boron levels as low as 200 wppm, which confirms very low solid solubility of B in Ti. TiB is typically found at the grain boundaries for minor boron additions, which would enhance the further processing by restricting the grain growth at high temperatures.

Scientific understanding of the influence of trace boron addition on the grain refinement of titanium alloys is studied in detail. An international journal article included in Attachment 1 describes these analyses.

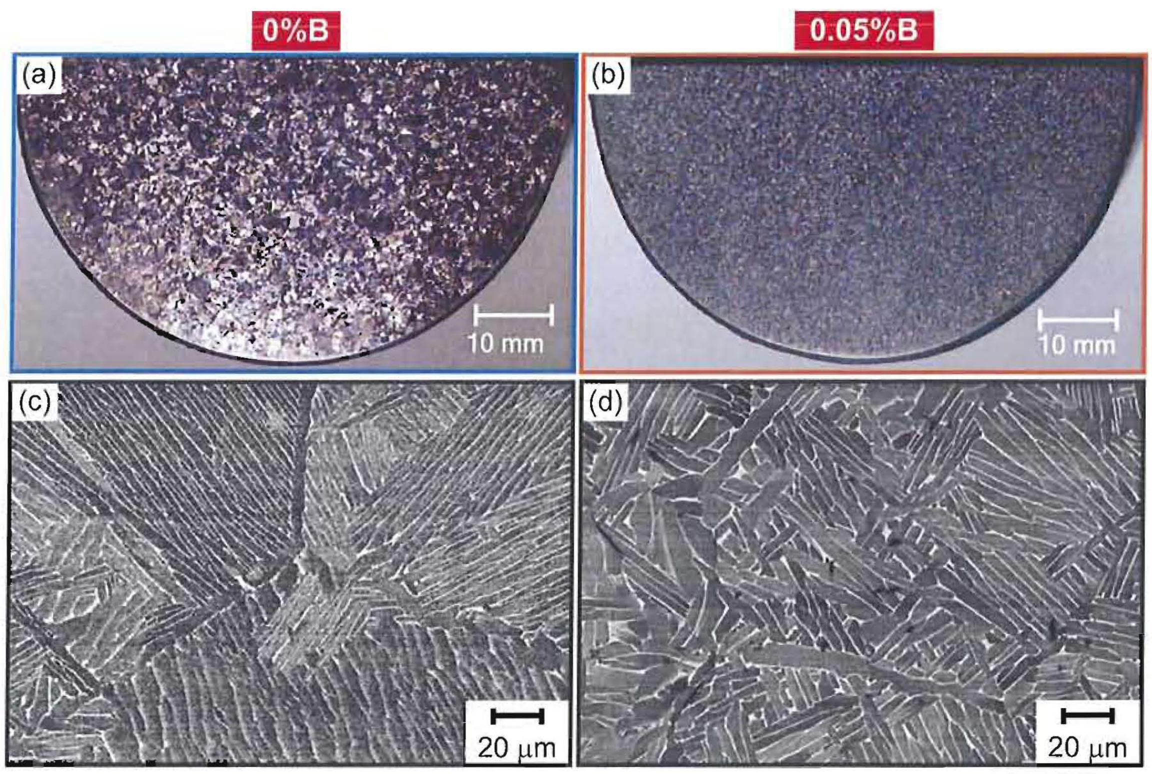

Fig. 1 (a,b) Macrographs and (c,d) backscattered electron images of as-cast Ti-64 with 0% B (a,c) and 0.05% B (b,d) showing the dramatic grain refinement due to boron addition.

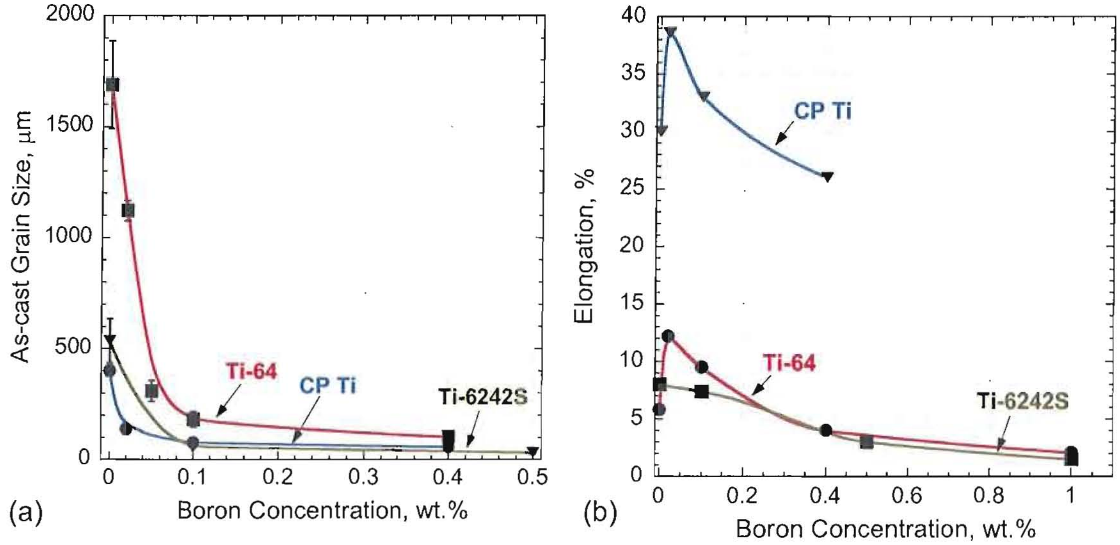

Fig. 2 Variation of Ti-64 (a) cast grain size and (b) room temperature elongation as a function of boron concentration in various cast Ti-B alloys.

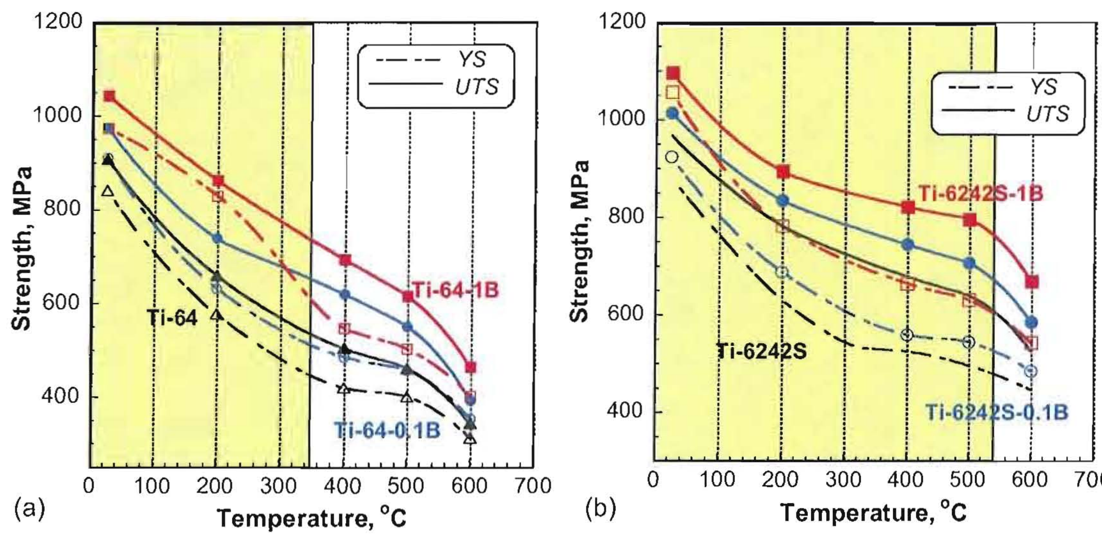

Fig. 3 Elevated temperature strengths (YS: yield strength, UTS: ultimate tensile strength) of as-cast Ti-B alloys (a) Ti-64-*x*B and (b) Ti-6242S-*x*B. The shaded temperature range corresponds to service temperature ranges of boron-free alloys.

5

Task 2: Development of Affordable Beta Titanium alloys

The development of next generation beta Ti alloys is expected to involve very attractive combinations of strength-toughness-fatigue resistance at large cross sections, improved and affordable processibility, and enhanced elevated temperature capability. This task describes the development of beta Ti alloys modified with small boron additions to achieve these goals. Detailed microstructural characterization and tensile property evaluation were conducted.

Two important aerospace metastable beta Ti alloys, Ti-15Mo-2.6Nb-3Al-0.2Si (Beta-21S) and Ti-5Al-5V-5Mo-3Cr (Ti-5553) Beta-21S and Ti-5553, micro alloyed (0.1%) with boron were produced using conventional melt processing route. Ingots of 70-mm diameter and 500-mm length were cast using induction skull melting and the influence of boron on the microstructures and tensile properties in the cast+HIP condition were established. The following conclusions are made based on the observations in this study.

- Beta Ti alloys modified with boron were successfully produced using a conventional casting method.
- Addition of 0.1% boron to Beta-21S and Ti-5553 significantly refines the cast grain size by a factor of ~5. Micro boron addition produces a cast grain size of ~50 μm, which is typically obtained after thermo-mechanical processing in the β phase field.
- Micro boron addition provides ~5% increase in strength and stiffness while maintaining good ductility.
- Strength enhancements due to boron addition to Ti-5553 are also maintained at elevated temperatures up to 400°C. Ability to retain higher strength enables better elevated temperature capability of beta Ti alloys.
- Micro boron addition enhances affordability of beta Ti alloys via grain refinement, enhanced mechanical properties, enhanced elevated temperature capability, and may also reduce the processing costs via reduction/elimination of thermo-mechanical processing steps.

An international journal article included in Attachment 1 provides complete description of this task.

6

Task 3: Affordable Superplastic Forming of Titanium Alloys"

The objective of this task is to explore affordable superplastic forming opportunities for titanium alloys. Small additions of boron to titanium alloys (Ti-B alloys) were considered in this task and superplastic forming (SPF) characteristics were evaluated.

Materials: A Ti-6Al-4V alloy with 1%B was produced via pre-alloyed powder metallurgy approach. Powder particles of Ti-64-1B were compacted at 1200°C and extruded at 1100°C. The microstructures of the extruded product (Fig. 1) exhibited nearly equiaxed α+β grain morphology with an average grain size of 5 μm. Presence of TiB is responsible for the evolution of equiaxed grain morphology even after processing well above the β transus of this alloy (~1000°C). The TiB whiskers aligned along the extrusion axis (Fig. 1a) and exhibited roughly hexagonal cross-sections (Fig. 1b). This is the starting material used for the evaluation of SPF characteristics. Room temperature tensile properties of this alloy were– modulus: 142 GPa, yield strength: 1079 MPa, ultimate strength: 1224 MPa, and elongation: 13%.

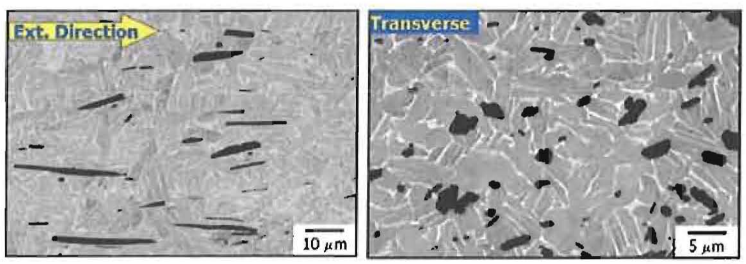

Figure 1 Microstructure of Ti-64-1B after extrusion (a) longitudinal and (b) transverse.

SPF Testing: ASTM proposed standard SPF test specimen geometry (Fig. 2, flat button-head sample of 25-mm gage length) and test procedure were used in this study. An MTS screw-driven test machine available in RG 2-4 was customized to establish in-house tensile testing capability under controlled atmosphere (vacuum/inert gas) up to 1400°C and at constant true strain rates in the range 10^{-5}–10^{-1} s^{-1}. TZM (molybdenum-based alloy) material was procured and grips were fabricated to perform testing using the existing setup.

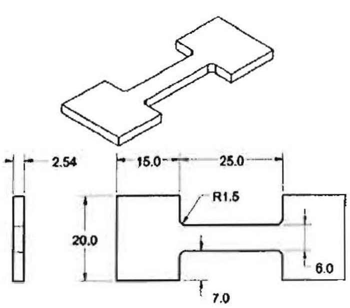

Fig. 2 Sample geometry used for SPF testing

Extruded Ti-64-1B alloy was tested at various temperatures in the range 800-1100°C and at a constant true strain rate of 10^{-3} s^{-1}. Superplastic flow behavior was observed around 900°C with a maximum elongation of 190% (Fig. 3). Additional testing at other strain rates (3×10^{-4} s^{-1}, 6×10^{-4} s^{-1}, and 10^{-2} s^{-1}) was also performed to establish the

7

strain rate influence on the SPF behavior. The starting microstructure appears to be not optimum for achieving best SPF performance. Process modifications are being considered to engineer the starting microstructural features that will enable improved SPF characteristics compared to conventional practices. Further refinement in grain size is likely to reduce the optimum SPF temperature and increase the strain rate, both of which are preferred in industrial SPF practice.

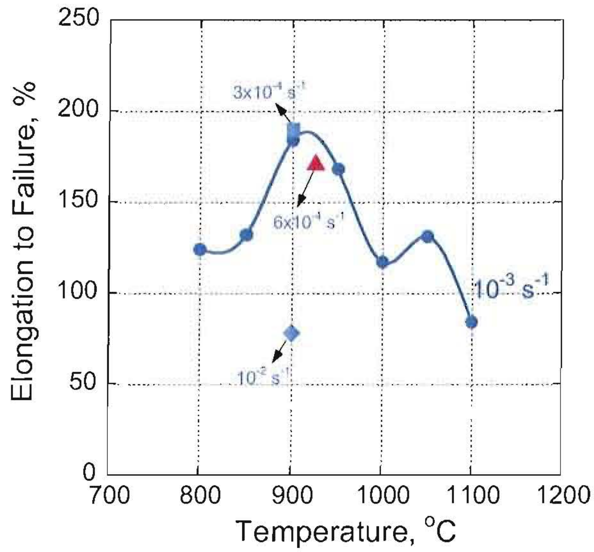

Fig. 3 Elongation of Ti-64-1B material as a function of temperature.

Fatigue Testing: Trace boron addition (0.05-0.1%) to Ti alloys produced an order magnitude reduction in cast grain size. Grain refinement significantly enhanced hot workability and enabled the ability to directly roll the cast stock without going through the intermediate process steps of ingot breakdown and conversion. Titanium components produced via SPF using these sheet stocks provide significant affordability benefits due to reduced process cost and lead-time. Production of sheet stock and evaluation of SPF characteristics of Ti-B alloy sheets is proposed for future work. To establish baseline fatigue properties for comparison, LCF S-N testing was performed on various cast+HIP Ti alloys with 0.1%B. The data (Fig. 4) shows that boron addition does not cause any debit in fatigue life.

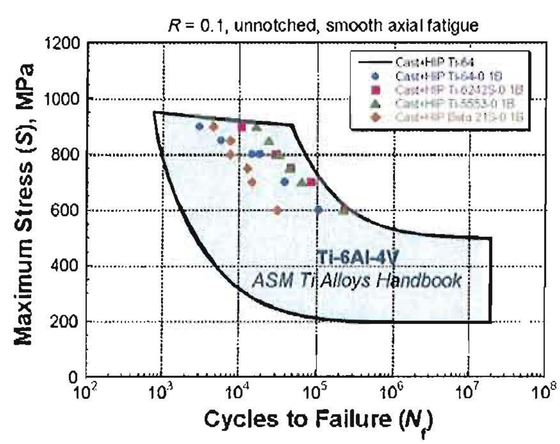

Fig. 4 Fatigue S-N data obtained on cast Ti alloys modified with 0.1B.

8

Task 4: Three-Dimensional Characterization of Ti-B Alloy Microstructures

This task was performed in collaboration with Georgia Institute of Technology. Three-dimensional (3D) microstructures of TiB phase in a powder metallurgy Ti–6Al–4V–1.7B alloy processed using two different routes are reconstructed from large-area high-resolution montage serial sections. Visualizations of the 3D microstructures are used to determine the effects of the processing route on the morphology, anisotropy, and spatial distributions of TiB particles. Complete microstructural analyses are provided in the publication included in Attachment 1.

A montage serial sectioning technique has been used to generate high-resolution (~ 0.5 μm), large-volume (0.13 mm3), 3D microstructures of a powder metallurgy Ti-6Al-4V-1B alloy containing TiB whiskers/particles in two different process conditions (blind die compacted, and blind die compacted and compacted and extruded). The visualization of the reconstructed 3D microstructure provides important insights on the 3D morphologies and distribution of fine eutectic TiB whiskers. In the as-compacted condition, the eutectic TiB whiskers have uniform random angular orientations, whereas after extrusion they tend to be aligned along the extrusion direction via rigid body rotation. Complete description of this effort is provided in the journal article included in Attachment 1.

Task 5: In situ Deformation Studies on Ti-B Alloys

This task was performed in collaboration with Michigan State University. In situ scanning electron microscopy was performed during both room temperature and 480°C tensile deformation of a boron modified Ti–6Al–4V alloy, in order to characterize the deformation evolution. The sequence of observable surface deformation events was: TiB whisker microcracking at stresses well below the global yield stress, multiple and extensive TiB cracking after global yielding, $\alpha + \beta$ phase slip emanating from the cracked TiB whiskers, localized shear band formation and propagation leading to cracking in the $\alpha + \beta$ phases, and ductile sample failure. TiB cracking was also observed throughout the subsurface locations on post-deformed samples. The early microcracking of TiB particles did not degrade mechanical properties, and higher tensile and ultimate strengths were obtained with a ductile fracture mode at quasi-static tensile elongations equivalent to conventional Ti–6Al–4V. Complete description of this task is provided in the journal article included in Attachment 1.

9

Attachment 1

Articles published in International Journals

1. Grain Refinement of Titanium Alloys via Trace Boron Addition
S. Tamirisakandala, R.B. Bhat, J.S. Tiley, and D.B. Miracle
Scripta Materialia, 53 (2005), pp. 1421-1426.

2. Processing, Microstructure, and Properties of Beta Titanium Alloys Modified With Boron
S. Tamirisakandala, R.B. Bhat, J.S. Tiley, and D.B. Miracle
Journal of Materials Engineering and Performance, 14, 6 (2005), pp. 741-746.

3. Reconstruction of three-dimensional microstructures of TiB phase in a powder metallurgy titanium alloy using montage serial sectioning
S. I. Lieberman, A.M. Gokhale, and S. Tamirisakandala
Scripta Materialia, 55 (2006), pp. 63-68.

4. In situ scanning electron microscopy observations of tensile deformation in a boron-modified Ti–6Al–4V alloy
C.J. Boehlert, C.J. Cowen, S. Tamirisakandala, D.J. McEldowney, and D.B. Miracle
Scripta Materialia, 55 (2006) pp. 465–468.

5. Reconstruction of Three-Dimensional Microstructures of TiB Whiskers in Powder Processed Ti-6Al-4V-1B Alloys
S. I. Lieberman, A.M. Gokhale, and S. Tamirisakandala
Materials Characterization, In Press

Available online at www.sciencedirect.com

SCIENCE DIRECT®

ELSEVIER

Scripta Materialia 53 (2005) 1421–1426

Scripta MATERIALIA

www.actamat-journals.com

Grain refinement of cast titanium alloys via trace boron addition

S. Tamirisakandala [a,b,*], R.B. Bhat [a,c], J.S. Tiley [a], D.B. Miracle [a]

[a] *Air Force Research Laboratory, Materials and Manufacturing Directorate, Bldg 655, 2230 Tenth Street, Wright-Patterson AFB, OH 45433, United States*
[b] *Department of Mechanical Engineering, Ohio University, Athens, OH 45701, United States*
[c] *UES, Inc., 4401 Dayton-Xenia Road, Dayton, OH 45432, United States*

Received 13 May 2005; received in revised form 27 July 2005; accepted 11 August 2005
Available online 12 September 2005

Abstract

The grain size of as-cast Ti–6Al–4V is reduced by about an order of magnitude from 1700 to 200 μm with an addition of 0.1 wt.% boron. A much weaker dependence of reduction in grain size is obtained for boron additions from >0.1% to 1.0%. Similar trends were observed in boron-modified as-cast Ti–6Al–2Sn–4Zr–2Mo–0.1Si.

Keywords: Titanium alloys; Casting; Grain refining; Microstructure

1. Introduction

Solidification is a dominant processing route for metallic materials, and grain refinement is of significant industrial importance. Fine grain size improves many mechanical properties such as strength, ductility, and damage tolerance, and enhances subsequent mechanical working response [1]. The grain sizes of conventional cast titanium alloys (e.g. Ti–6Al–4V) are rather coarse (from several millimeters to centimeters depending on cast billet size) due to rapid coarsening in the body-centered cubic β phase and the grain size typically increases with an increase in section thickness (i.e. decrease in cooling rate) [2]. Extensive thermo-mechanical processing is essential to breakdown the cast structure and texture in order to obtain a good balance of static and dynamic property combinations [3], but this is expensive and adds significantly to the time required to produce high quality titanium billets. Addition of inoculants to many molten metal alloys is the most commonly used commercial practice to achieve grain refinement via acceleration of the heterogeneous nucleation rate [4]. Some examples include addition of trace boron (~5 ppm) to Al alloys, impure ferrosilicon to cast iron, and Zr to certain Mg alloys. The inoculation leads to a dispersion of stable, insoluble solid particles in the melt on which grains nucleate.

No grain refinement mechanism via inoculation is reported for conventional Ti alloys. Recently Zhu et al. [5] considered addition of a small amount (<0.5%) of boron to cast Ti alloys with the motivation of enhancing mechanical properties for dental applications and they observed significant grain refinement. The microstructural refinement was attributed to the precipitation of TiB particles, which is not likely since the TiB phase precipitates out after the formation of primary β_{Ti} grains for these compositions according to the well-established Ti–B phase diagram [6] shown in Fig. 1. The alloys studied by Zhu et al. were cast in the form of very small size ($45 \times 20 \times 12$ mm^3) button ingots using a dental casting machine, and significant oxygen contamination was reported [5], which could play an important role on the solidification characteristics. While this earlier work provides the first important observation of grain refinement of cast Ti alloys by small boron

* Corresponding author. Address: Air Force Research Laboratory, Materials and Manufacturing Directorate, Bldg 655, 2230 Tenth Street, Wright-Patterson AFB, OH 45433, United States. Tel.: +1 937 904 4333; fax: +1 937 255 3007.
E-mail address: sesh.tamirisa@fnnet.wpafbml.org (S. Tamirisakandala).

1359-6462/$ - see front matter © 2005 Acta Materialia Inc. Published by Elsevier Ltd. All rights reserved.
doi:10.1016/j.scriptamat.2005.08.020

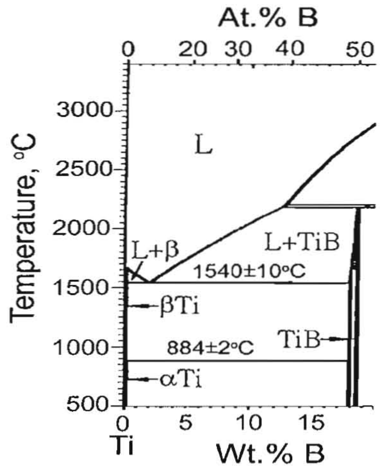

Fig. 1. Titanium-rich section of binary Ti–B phase diagram (from Ref. [6]).

additions, a number of important details such as quantified assessment and conclusive understanding of the boron effect were not adequately addressed.

The principal objective of the present work was to determine the influence of boron addition on grain refinement in conventional Ti alloys. A second objective was to develop insight into the mechanism of grain refinement of Ti alloys via boron addition. To meet these objectives, systematic studies were conducted using Ti alloy ingots produced via a commercially established ingot metallurgy process and detailed microstructural analyses.

2. Experimental

Two widely used Ti alloys, Ti–6Al–4V (referred to hereafter as Ti-64) and Ti–6Al–2Sn–4Zr–2Mo–0.1Si (referred to hereafter as Ti–6242S) were considered in this study (all compositions are expressed in weight per cent). Ingots from each of these compositions alloyed with various boron levels in the range 0.02–1% were melted at Flowserve Corporation, Dayton, OH in an induction skull melting chamber and cast into graphite molds. The cast ingot dimensions were 70 mm diameter × 500 mm length. The boron was added in the form of elemental boron that completely dissolved in the liquid melt. Ingots of boron-free Ti-64 and Ti–6242S were also prepared using the same melting and casting procedure for comparison purposes. All the ingots were subjected to a standard hot isostatic pressing (HIP) treatment at 900 °C and 100 MPa for 2 h [7]. During HIP, the material plastically deforms, closing internal shrink cavities and diffusion bonding the cavity surfaces. Since the HIP temperature is well below the β transus temperature (~1000 °C), the microstructural features of as-cast and cast + HIP will be essentially identical, except for the absence of porosity in the latter [2]. The ingots were radiographed after HIP and confirmed to be free from porosity. The ingots were sectioned along the transverse cross section and samples were ground, polished, and subsequently chemically etched with Kroll's reagent (2%HF + 4%HNO_3 + distilled water) to expose the microstructures. The cast (i.e. prior β) grain sizes were measured using the linear intercept method [8]. Microstructural observations were made on unetched specimens using a light microscope under polarized light and field-emission high-resolution scanning electron microscope in the backscattered electron imaging mode. The constituent phases were identified via X-ray diffraction.

3. Results

Chemical analyses of the Ti alloy ingots considered in this study are given in Table 1. The cast grain morphologies of all the Ti-64 and Ti–6242S castings were equiaxed and the grain sizes of boron-free alloys were coarse. Macrographs recorded on transverse sections of Ti-64 and Ti-64–0.06B ingots are shown in Fig. 2, which illustrate the dramatic grain refinement produced by the trace boron addition. Polarized light micrographs of Ti-64 and Ti–6242S alloys without and with boron shown in Fig. 3 reveal that fine grain size also produces fine α + β lamellar colonies in the grain interiors. The variation of grain size of Ti-64 and Ti–6242S alloys with boron concentration is plotted in Fig. 4. Addition of 0.1% boron refines the Ti-64 average grain size from 1700 to 200 μm and the Ti–6242S average grain size from 550 to 50 μm. The grain size versus boron concentration curves possess a knee in the range 0.06–0.1%B, which indicates that there exists a

Table 1
Chemical compositions (in wt.%) of boron modified Ti alloys used in the study

Alloy	Al	V	Sn	Zr	Mo	Si	B	O	H	C	N	Fe	Ti
Ti-64	6.6	4.1					–	0.18	0.008	0.02	0.01	0.23	Balance
Ti-64–0.02B	6.0	4.0					0.02	0.13	0.005	0.02	0.01	0.14	Balance
Ti-64–0.06B	6.7	4.1					0.06	0.17	0.005	0.02	0.02	0.21	Balance
Ti-64–0.1B	6.0	4.0					0.10	0.15	0.005	0.02	0.01	0.13	Balance
Ti-64–0.4B	6.0	4.1					0.41	0.16	0.009	0.02	0.01	0.15	Balance
Ti-64–1.0B	5.9	4.0					0.98	0.18	0.009	0.02	0.02	0.13	Balance
Ti–6242S	5.8		2.0	4.1	2.0	0.08	–	0.15	0.001	0.01	0.004	0.07	Balance
Ti–6242S–0.1B	6.0		2.0	4.0	2.1	0.09	0.09	0.14	0.007	0.01	0.01	0.04	Balance
Ti–6242S–0.4B	5.9		1.9	4.0	2.0	0.10	0.44	0.16	0.004	0.02	0.01	0.05	Balance
Ti–6242S–1.0B	5.9		1.9	4.1	2.0	0.11	0.92	0.18	0.008	0.01	0.01	0.05	Balance

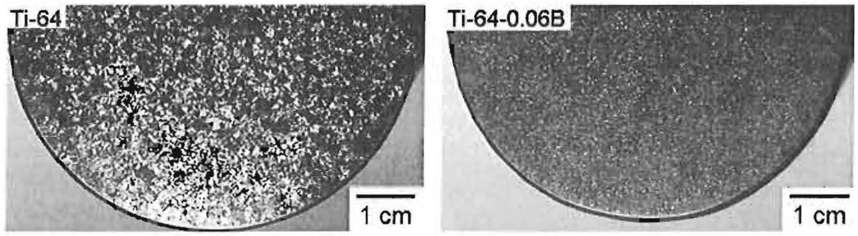

Fig. 2. Macrographs of the transverse cross sections of cast Ti-64 and Ti-64–0.06B ingots.

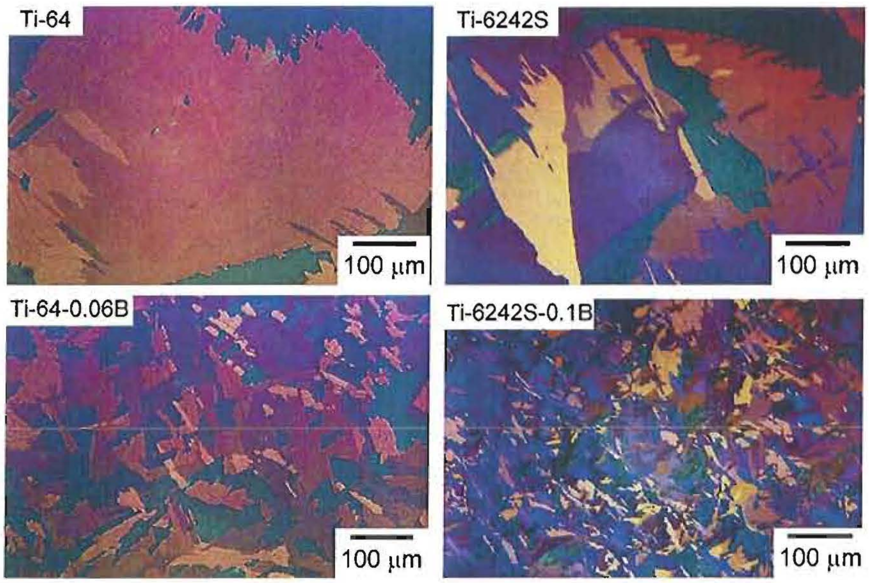

Fig. 3. Polarized light micrographs obtained on cast Ti-64 and Ti-6242S illustrating the influence of trace boron addition on the colony structure within the prior β grains.

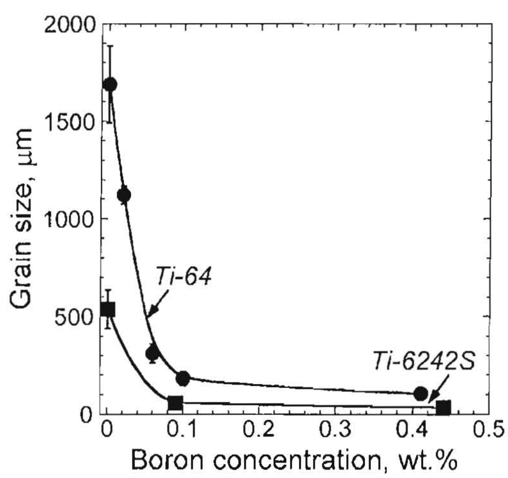

Fig. 4. Variation of cast grain size of Ti-64 and Ti-6242S with boron concentration.

critical level of boron required for obtaining dramatic grain refinement, beyond which only a small additional reduction in grain size is obtained. Coarse prior β grain boundaries are not present in alloys containing 1% boron and hence no prior β grain size is reported.

Backscattered electron images of Ti-64 containing various boron levels are presented in Fig. 5. In general, both the prior β grain size and α–β colony size decrease as the boron level increases. At 0.02% boron, equiaxed TiB particles of 0.1 vol.% are present (Fig. 5(b)), which confirms that the solid solubility of boron in Ti-64 is below this level. The TiB adopts a needle morphology and forms a necklace structure at the prior β grain boundaries for 0.1% boron additions (Fig. 5(d)). The needle morphology is retained at 0.4% and 1.0% boron, but the distribution of TiB becomes more uniform (Fig. 5(e) and (f)). Similar trends are observed for Ti-6242S with increasing boron levels (Fig. 6).

4. Discussion

Although phase diagrams for multicomponent Ti alloys with boron are not yet established, the binary Ti–B phase diagram (Fig. 1) provides a reasonable guide to understanding the solidification sequence and microstructural development of the alloys studied. In hypoeutectic Ti–B alloys, primary β_{Ti} grains nucleate and grow upon cooling between the liquidus and the eutectic temperatures (Fig. 1). Below the eutectic temperature, the remaining liquid

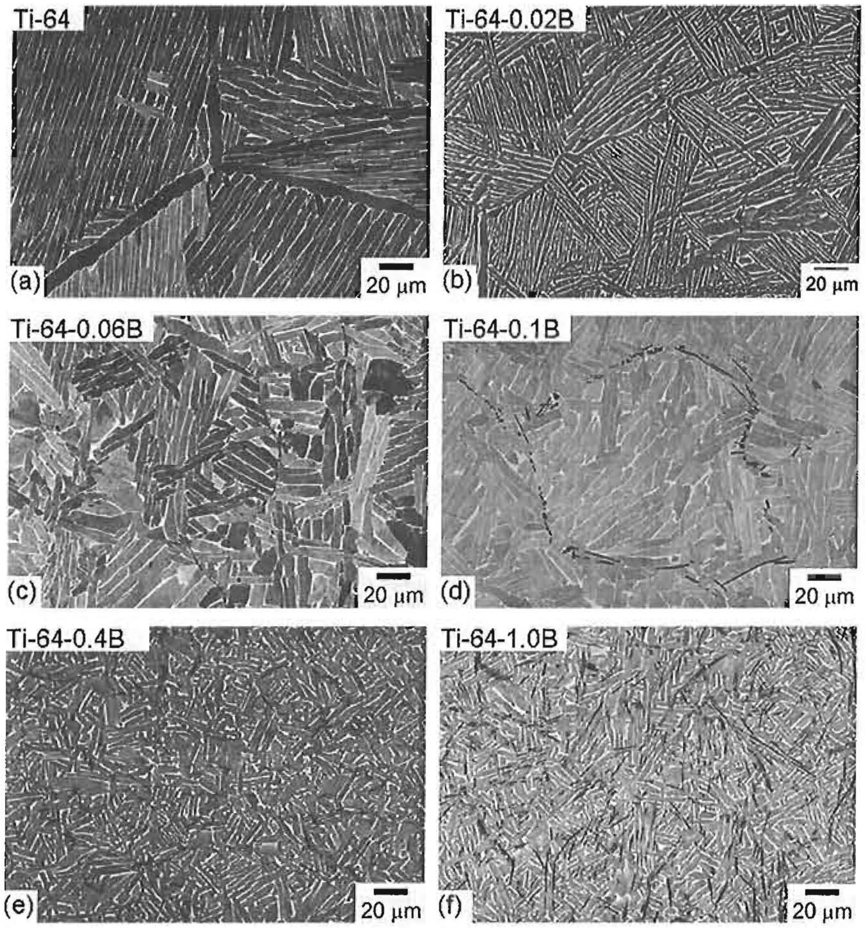

Fig. 5. Backscattered electron images of cast Ti-64 containing boron levels indicated on the micrographs. The gray background is the α, bright phase is the β, and dark black phase is the TiB.

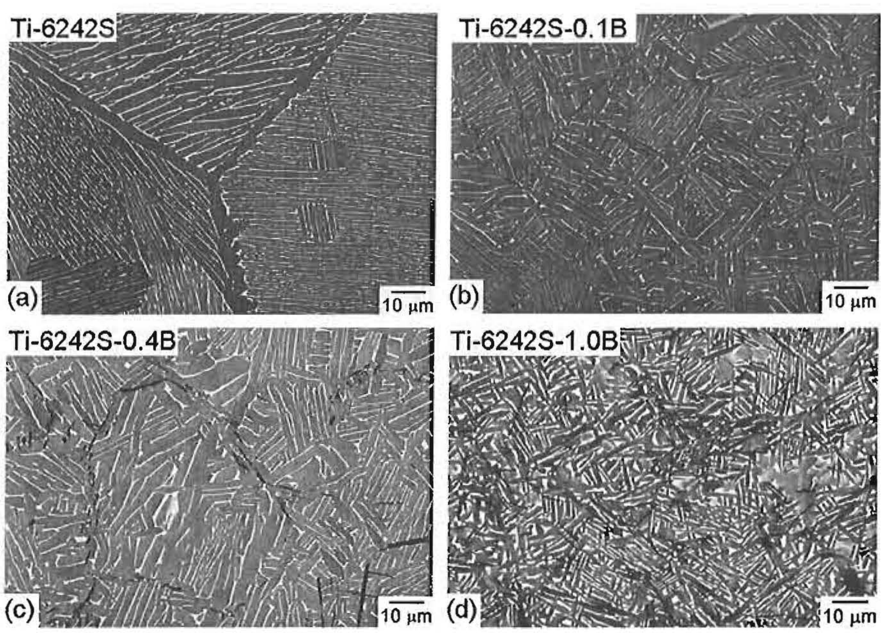

Fig. 6. Backscattered electron images of Ti–6242S with boron levels indicated on the micrographs.

trapped between the β_{Ti} grains solidifies via the eutectic reaction, forming an irregular eutectic mixture of $\beta_{Ti}+$ TiB. Cooling below the β transus motivates the $\beta \rightarrow \alpha$ allotropic transformation as in conventional Ti alloys, and the prior β grain boundaries are retained in the microstructures observed at room temperature. Since the TiB forms after the primary β_{Ti} in hypoeutectic compositions, the TiB particles cannot act as nucleation sites for the formation of β_{Ti} grains and grain refinement via inoculation is not expected to occur. In view of this, an alternate grain refinement mechanism is necessary to explain the experimental observations.

The grain size obtained after solidification is determined by competition between the nucleation and growth rates. Trace boron additions are likely to enhance the nucleation rate by providing additional driving force and/or slowing the growth rate by influencing the liquid/solid interfacial characteristics. Although more fundamental calculations and/or instrumented experiments are necessary to ascertain the exact grain refinement mechanism via trace boron addition, the following possibilities are proposed to explain the results obtained in this study.

The appearance of equiaxed grains throughout the billet cross sections in all of the castings implies that supercooling arising from a change in composition (constitutional) is more important during solidification than thermal undercooling. The solid solubility of boron in elemental titanium has been established to be below 0.02% [9], and the presence of TiB in Ti-64 containing 0.02%B in this study extends this result to titanium alloys (Fig. 5(b)). Thus, boron is rejected from the primary β_{Ti} nuclei into the melt, producing solute partitioning into the liquid ahead of the solidification front. This solute enrichment causes a corresponding variation in the liquidus temperature leading to higher constitutional supercooling (CS). As solidification progresses, CS causes instability at the liquid/solid interface and provides an additional driving force for the nucleation of more fine β_{Ti} grains ahead of the solid/liquid interface.

Once a nucleus is formed, its growth is influenced by kinetics of atom attachment to the interface, capillarity, and diffusion of heat and mass at the interface and away from the interface. The boron rejected at the solid/liquid interface is likely to influence these factors and restrict the growth of existing nuclei. The excess boron rejected from the solid will accumulate in an enriched boundary layer ahead of the interface [10]. At boron concentrations below a critical value (~0.06%), the rejected boron ahead of the interface can be dispersed readily into the remaining liquid and significant grain refinement is not achieved. When critical amount of boron is present in the melt, boron-rich layer retards the growth of the nuclei thereby allowing more nuclei to form in the surrounding supercooled melt, leading to a fine grain size.

The degree of grain refinement relies on the balance between latent heat production and heat extraction at the solid/liquid interface. The rate of latent heat production is limited by the solute partitioning at the solid/liquid interface and diffusion in the melt. For idealized binary systems, Maxwell and Hellawell [11] proposed that diffusion-limited growth rate of a sphere at a given melt undercooling and sphere radius is inversely proportional to the thermodynamic quantity

$$Q = m(k-1)C_0 \tag{1}$$

where m is the slope of the liquidus, k is the solute partition coefficient ($=C_S/C_L$, where C_S and C_L are the solute contents of the solid and liquid in equilibrium at the interface between them) and C_0 is the solute content. The basis of the Maxwell–Hellawell model [11] is that restriction of the growth of already nucleated grains permits continuing nucleation in the undercooled melt until the total latent heat release is sufficient to cause recalescence and the loss of undercooling. The growth-restriction factor Q is a good parameter to describe the solute effects on grain refinement and characterizes the degree of growth restriction for a small undercooling set independently. It has been shown [4] that the overall Q in multicomponent alloys is the sum of Q values for the individual solutes. The variation of Q calculated for binary Ti–B with the measured grain sizes of boron-modified Ti-64 and Ti-6242S alloys is shown in Fig. 7. Good correlation between grain size and Q for given refining conditions indicates the influence of boron on growth restriction and the variation closely follows the trends of grain refinement observed in Al alloys [4].

Grain refinement is expected to improve with an increase in boron level due to higher CS but the experimental observations reveal a saturation in the grain size with boron content and absence of coarse prior β grains at 1% B level (Figs. 5(f) and 6(d)). This trend of a rapid decrease at first, followed by saturation, is predicted from the variation of grain size versus Q [4] and the present observations match with these predictions. Further, in hypoeutectic alloys, the volume fraction of primary β_{Ti} decreases and eutectic β_{Ti} increases with increase in boron

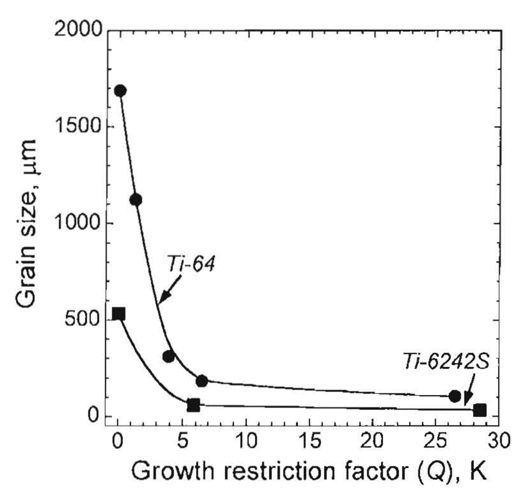

Fig. 7. Measured grain sizes of boron-modified Ti-64 and Ti–6242S alloys as a function of growth-restriction factor Q (Eq. (1)).

concentration towards the eutectic limit. The eutectic β_{Ti} precipitates at a finer length scale and coarsening rate would be much slower than that of primary β_{Ti}.

Addition of a critical amount of boron to near-γ titanium aluminides has been reported [12] to produce grain refinement in as-cast microstructures similar to that of conventional Ti alloys observed in this study. A hypothesis based on nucleation in the constitutionally supercooled zone ahead of the solidification front was put forward to explain the grain refinement phenomenon caused by boron addition to γ-TiAl alloys [12]. The grain refinement process in these alloys was suggested as a dynamic equilibrium between solute rejection at the solidification front, the formation of borides, and alloy nucleation ahead of the front. The mechanism of grain refinement in conventional Ti alloys proposed in this paper appears to be somewhat similar to that proposed in γ-TiAl alloys in terms of constitutional supercooling although differences exist in solidification sequences and influence of boron on growth rate.

The TiB precipitates may play an important role in the microstructural refinement during subsequent thermal exposure of the cast microstructure to temperatures above the β transus. The phase transformation from β to α occurs by nucleation and growth according to Burger's orientation relationships and presence of TiB could enhance the kinetics of this phase transformation by providing additional nucleation sites. Hill et al. [13] have observed the precipitation of equiaxed α instead of lamellar α in the as-cast Ti-64–2B after slow-cooling from above the β transus without imposing any mechanical work in the $\alpha + \beta$ phase field. TiB particles could also enhance microstructural stability during subsequent thermal exposure at elevated temperature by restricting the mobility of grain boundaries via Zener pinning [14].

5. Conclusions

Trace boron addition (~0.1 wt.%) to Ti–6Al–4V produces a reduction in the as-cast grain size by roughly an order of magnitude compared to boron-free alloy. Experimental results revealed a much weaker dependence of reduction in grain size for boron additions higher than 0.1%. Similar trends were observed in the alloy Ti–6Al–2Sn–4Zr–2Mo–0.1Si. Grain refinement of cast Ti alloys via boron addition and criticality of the boron concentration on the extent of grain refinement are hypothesized as effects of constitutional supercooling, caused by the boron rejected from the primary β_{Ti} grains into the liquid ahead of the solidification front and its influence on the nucleation and growth rates.

Acknowledgements

Financial support for this research was provided by the AFRL/ML Lab Director's Funds. ST is supported under the auspices of Air Force Contract F33615-03-D-5801. The authors acknowledge useful discussions with Drs. O.M. Ivasishin and M.H. Loretto.

References

[1] Flemings MC. Solidification Processing. New York, NY: McGraw-Hill; 1974. p. 341.
[2] Eylon D, Newman JR, Thorne JK. Metals Handbook, vol. 2. Materials Park, OH: ASM International; 1991. p. 634.
[3] Terlinde G, Witulski T, Fischer G. In: Leyens C, Peters M, editors. Titanium and titanium alloys. Weinheim: Wiley-VCH; 2003. p. 289.
[4] Greer AL, Cooper PS, Meredith MW, Schneider W, Schumacher P, Spittle JA, et al. Adv Eng Mater 2003;5:81.
[5] Zhu J, Kamiya A, Yamada T, Shi W, Naganuma K. Mater Sci Eng A 2003;339:53.
[6] Marray JL, Liao PK, Spear KE. In: Baker H, editor. Binary alloy phase diagrams. Materials Park, OH: ASM International; 1992. p. 285.
[7] Magnuson J. Metallography 1977;10:223.
[8] E112-96e2. In: ASTM book of standards. Philadelphia, PA: ASTM; 2004. vol. 03.01.
[9] Palty AE, Margolin H, Nielsen JP. Trans ASM 1954;46:312.
[10] Kurz W, Fisher DJ. Fundamentals of solidification. Switzerland: Trans Tech; 1984. p. 51.
[11] Maxwell I, Hellawell A. Acta Metall 1975;23:229.
[12] Cheng TT. Intermetallics 2000;8:29.
[13] Hill D, Banerjee R, Huber D, Tiley J, Fraser HL. Scripta Mater 2005;52:387.
[14] Zener C. quoted in Smith CS. Trans Met Soc AIME 1948;175: p. 15.

JMEPEG (2005) 14:741-746
DOI: 10.1361/105994905X75547

1059-9495/$19.00

Processing, Microstructure, and Properties of β Titanium Alloys Modified With Boron

Seshacharyulu Tamirisakandala, Radhakrishna B. Bhat, Jaimie S. Tiley, and Daniel B. Miracle

(Submitted August 24, 2005)

The development of next-generation βTi alloys is expected to involve very attractive combinations of strength-toughness-fatigue resistance at large cross sections, improved and affordable thermomechanical processing, and enhanced elevated temperature capability. This article describes the development of βTi alloys that are modified with small boron (B) additions to achieve these goals. Two important aerospace alloys, Ti-15Mo-2.6Nb-3Al-0.2Si and Ti-5Al-5V-5Mo-3Cr microalloyed (0.1%) with B were considered. Ingots that were 70 mm in diameter and 500 mm in length were cast using induction skull melting. A detailed microstructural characterization and tensile property evaluation were conducted. Microalloying with B refines the cast grain size to about 50 μm, which enhances strength and ductility. The effect of B additions on the microstructural stability and properties in the as-cast condition was established. The implications of B additions on the microstructural evolution and affordability of subsequent processing is also discussed.

Keywords β titanium alloys, B addition, cast alloys, microstructure, properties

1. Introduction

Beta Ti alloys are the most versatile class of Ti alloys offering a wide range of processing and physical-chemical-mechanical property combinations compared with any other class of Ti alloys (Ref 1). Despite this wide range of attributes, there were very few applications of β alloys in the early 1990s, accounting for only 1% of the total Ti market (Ref 2). In the past, the majority of the development of β alloys has been driven by performance, and the high cost factor has slowed down the integration of βTi alloys. The usage of βTi alloys has increased significantly in the last 10 years due to the focused effort in reducing the formulation and processing costs (Ref 3). Currently, βTi alloys are widely used in aerospace, automotive, biomedical, and sporting applications (Ref 1). More widespread use and the justification to replace existing materials with β alloys are envisaged if affordable processing methodologies are developed and adopted (Ref 2). The most important microstructural parameters that control the properties of βTi alloys are prior β grain size, the primary and secondary α, including their volume fraction, morphology, size, and distribution, and the grain boundary α morphology and volume fraction. Innovations in processing are the key to enhancing the affordability of β alloys while obtaining controlled microstructures. Titanium alloys modified with boron (B) are emerging as a new class of alloys with exceptional promise for achieving this goal (Ref 4, 5). Boron, unlike other interstitial elements such as oxygen and hydrogen, is almost insoluble in Ti in the solid state (Ref 6) and, thus, does not embrittle the lattice. Recent studies have demonstrated that micro-B additions to conventional $\alpha + \beta$ Ti alloys (Ti-6-4 and Ti-6-2-4-2S) produced dramatic (by a factor of 10) grain refinement in the as-cast condition (Ref 7). The optimum B concentration (i.e., in the range 0.05-0.1%) was established for producing an order of magnitude grain refinement in these alloys. The objectives of this research effort are to understand the effect of micro-B additions on the microstructural evolution and the mechanical properties of βTi alloys and to explore the influence of B additions on the affordability of βTi alloys.

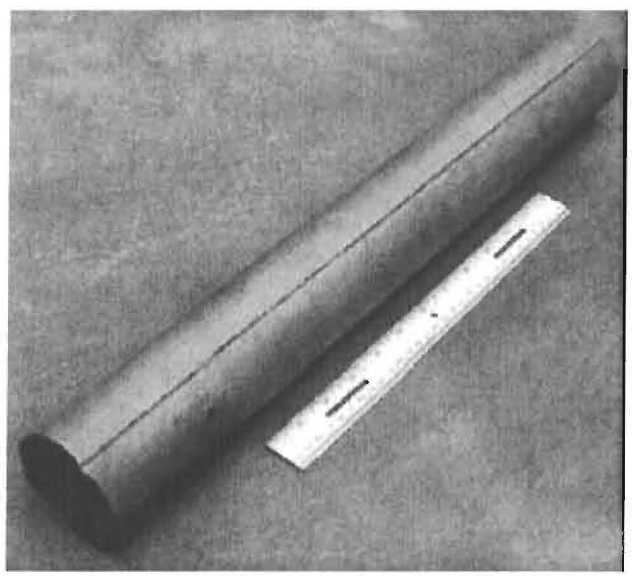

Fig. 1 Photograph of a typical βTi alloy cast ingot produced via induction skull melting

This paper was presented at the Beta Titanium Alloys of the 00's Symposium sponsored by the Titanium Committee of TMS, held during the 2005 TMS Annual Meeting & Exhibition, February 13-16, 2005 in San Francisco, CA.

Seshacharyulu Tamirisakandala, Department of Mechanical Engineering, Ohio University, Athens, OH 45701; **Radhakrishna B. Bhat,** UES Inc., 4401 Dayton-Xenia Road, Dayton, OH 45432; and **Jaimie S. Tiley** and **Daniel B. Miracle,** Air Force Research Laboratory, Materials and Manufacturing Directorate, Wright-Patterson AFB, OH 45433. Contact e-mail: sesh.tamirisa@fnnet.wpafbml.org.

2. Experimental

2.1 Materials

Two metastable βTi alloys with nominal compositions of Ti-15Mo-2.6Nb-3Al-0.2Si (Beta-21S) and Ti-5Al-5V-5Mo-3Cr (Ti-5553) were considered in this study. Each of these compositions without and with 0.1% B were produced at Flowserve Corporation, Dayton, OH, via induction skull melting using graphite molds. The B was added in the form of elemental B that completely dissolves in the liquid melt and forms TiB precipitates in situ during solidification. The cast ingot dimensions were 70 mm in diameter × 500 mm in length. All of the ingots were subjected to hot isostatic pressing (HIP) at 900 °C and 100 MPa for 2 h. After HIP, the ingots were radiographed and were confirmed to be free from porosity. A photograph of a typical ingot is shown in Fig. 1, and complete chemical analyses of the program materials are presented in Table 1.

2.2 Metallography

Samples for microstructural examination were cut from the cast ingots, prepared by standard polishing techniques, and observed using both light microscopy (LM) and scanning electron microscopy (SEM). Polarized light was used for observations in LM, and the backscattered electron imaging mode was used in SEM. The grain sizes of the cast microstructures were measured using the linear intercept method.

2.3 Tensile Testing

Round threaded tensile specimens with a 5 mm gage diameter and 30.5 mm gage length were prepared via electric discharge machining and low-stress grinding. Tensile testing was performed according to ASTM standard E08 using a servohydraulic test frame. A 20 mm extensometer was used in the gage portion to measure the strain during room temperature testing, and the samples were pulled at a constant crosshead speed of 0.01 mm/s. Tests were also conducted at elevated temperatures up to 400 °C for the Ti-5553 alloys. The fracture surfaces of selected specimens were observed with SEM using secondary electron imaging.

3. Results and Discussion

3.1 Microstructures

Polarized light micrographs of the as-polished specimens of Beta-21S and Beta-21S-0.1B are shown in Fig. 2(a) and (b), respectively, which clearly illustrate the grain refinement effect caused by B addition. The grain size measurements revealed that the addition of 0.1 B refines the average cast grain size (or prior β grain size) from 150 to 50 μm. Backscattered electron images of the Beta-21S and Beta-21S-0.1B alloys are presented in Fig. 3, which reveal the morphology and finer structural details of the microconstituents. Beta-21S without B exhibits coarse prior β grains (Fig. 3a) that are decorated with a thin and continuous grain boundary α film (Fig. 3b) of approximately 0.5 μm width. Beta-21S-0.1B, on the other hand, exhibits fine grains (Fig. 3c) with grain boundary α as small platelets (Fig. 3d). The addition of 0.1 B produces TiB in situ, which is preferentially located at the grain boundaries (Fig. 3d). In both of the alloys, the intragranular structure consisted of acicular α in the β matrix, which is typically observed after the solution treatment of Beta-21S above the β transus (~810 °C) (Ref 8).

Polarized light micrographs of the Ti-5553 and Ti-5553-

Table 1 Chemical analysis of the cast βTi-B program materials

Alloy	Mo	Nb	Al	Si	Fe	B	O	H	N	C	Ti
β-21S	15.2	2.8	2.7	0.2	0.43	...	0.19	0.0007	0.022	0.02	bal
β-21S-0.1B	14.7	2.8	2.8	0.2	0.41	0.12	0.20	0.0008	0.022	0.02	bal
		V		**Cr**							
Ti-5553	5.2	5.0	5.1	3.0	0.4	...	0.21	0.0014	0.01	0.02	bal
Ti-5553-0.1B	5.0	4.9	5.2	3.2	0.5	0.1	0.19	0.0008	0.01	0.01	bal

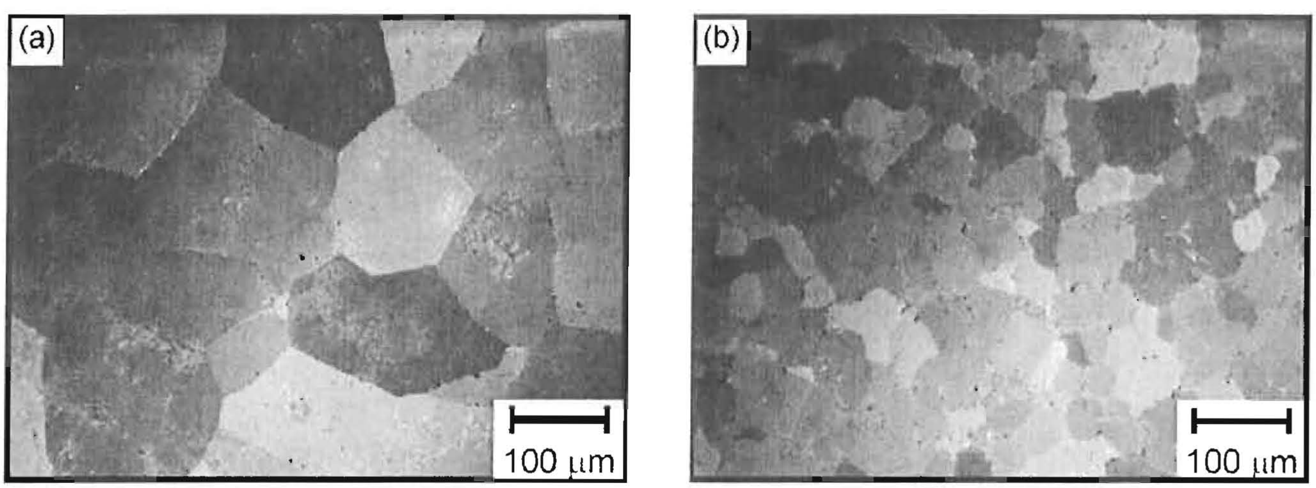

Fig. 2 Polarized light micrographs of the as-polished specimens of (a) Beta-21S and (b) Beta-21S-0.1B

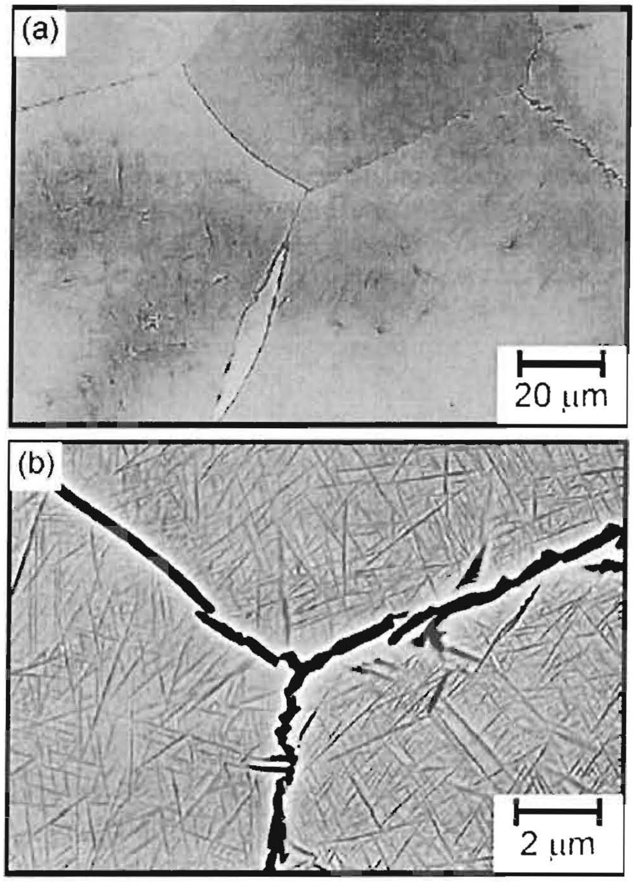

Fig. 3 Backscattered electron images of the as-polished specimens of (a, b) Beta-21S and (c, d) Beta-21S-0.1B. (a, c) are at low magnification, and (b, d) are at high magnification. The contrast of the micrograph (d) was digitally enhanced to reveal the difference between grain boundary α (gray) and TiB (black).

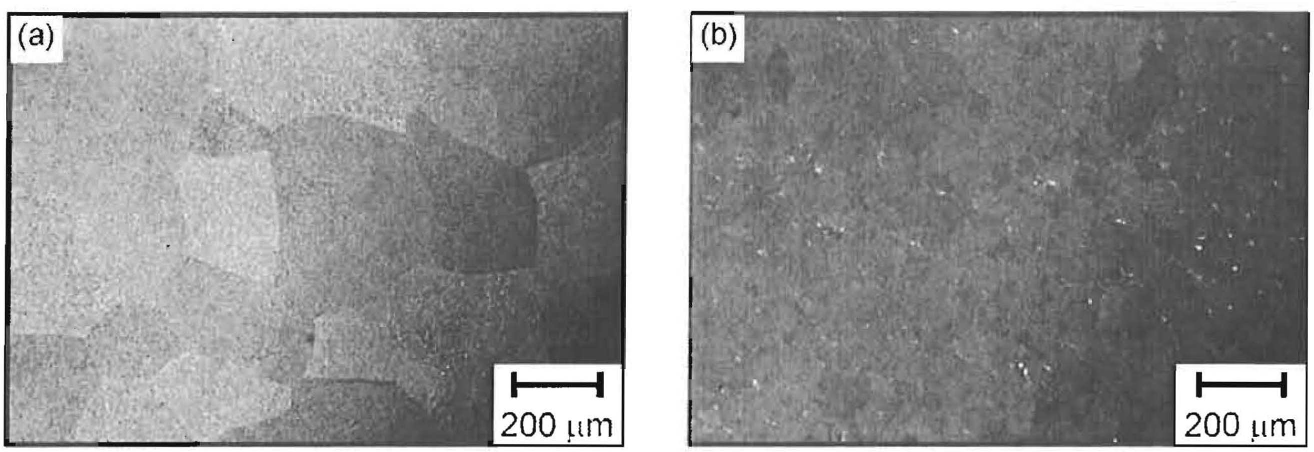

Fig. 4 Polarized light micrographs of the as-polished specimens of (a) Ti-5553 and (b) Ti-5553-0.1B

0.1B alloys shown in Fig. 4 illustrate the dramatic grain refinement effect of B, which is similar to that of Beta-21S. The average cast grain size was refined from 350 to 50 μm due to micro-B addition to Ti-5553. Backscattered electron images of these alloys at low and high magnifications are presented in Fig. 5. The Ti-5553 alloy modified with B exhibits fine prior β grains (Fig. 5c) with discontinuous grain boundary α and fine TiB precipitates at the grain boundaries. The grain interior structure in both of the alloys is acicular α in the β matrix, which is typical of the β solution-treated condition (Ref 8).

Grain refinement improves many of the metallurgical properties such as strength, ductility, and fatigue life, while mitigating the tendency for cracking and slowing the crack growth rate. Typically, Ti alloys are subjected to extensive thermomechanical processing (TMP) to refine the microstructure (Ref 1, 8). The ability to obtain fine grain sizes in the as-cast condition

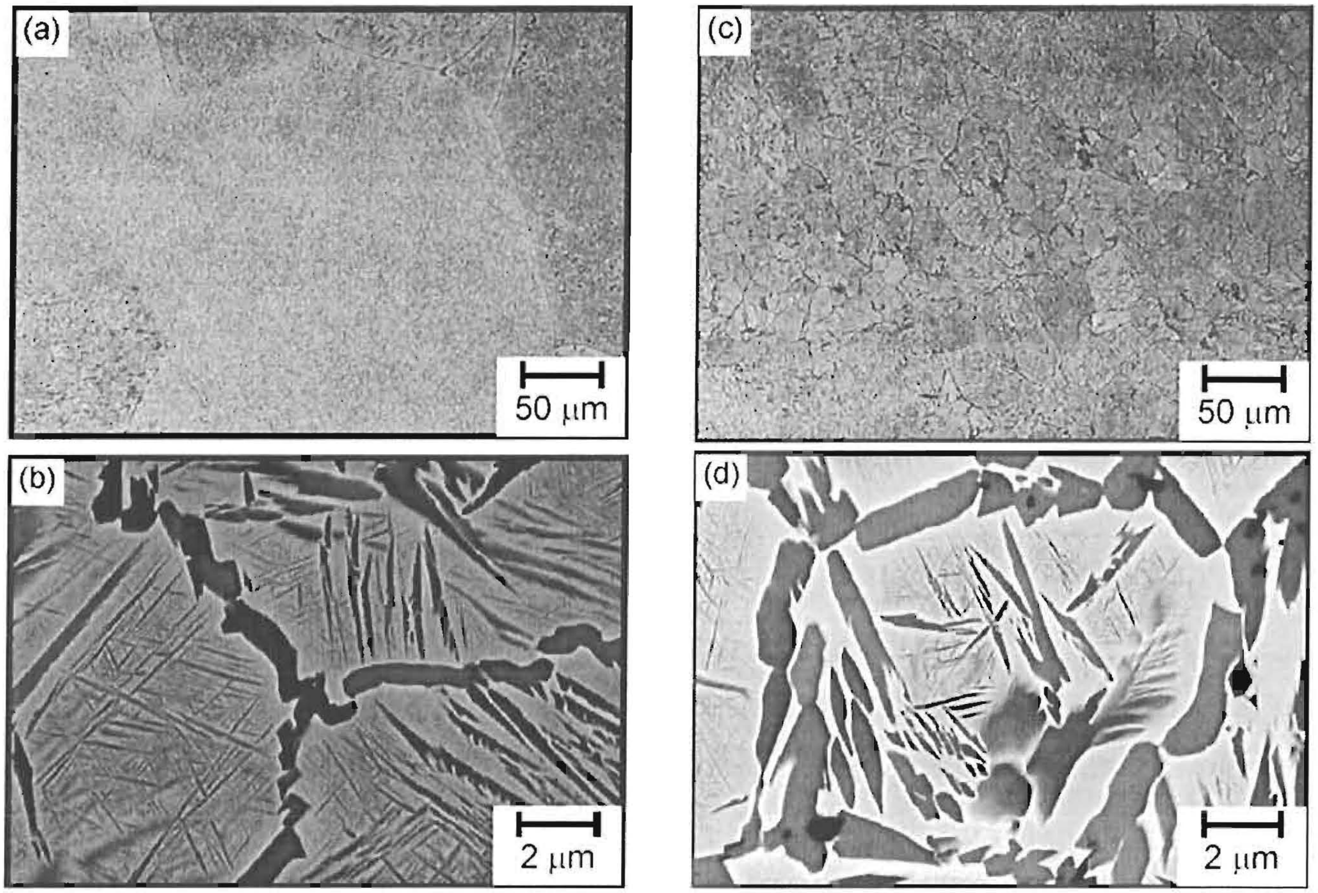

Fig. 5 Backscattered electron images of the as-polished specimens of (a, b) Ti-5553 and (c, d) Ti-5553-0.1B

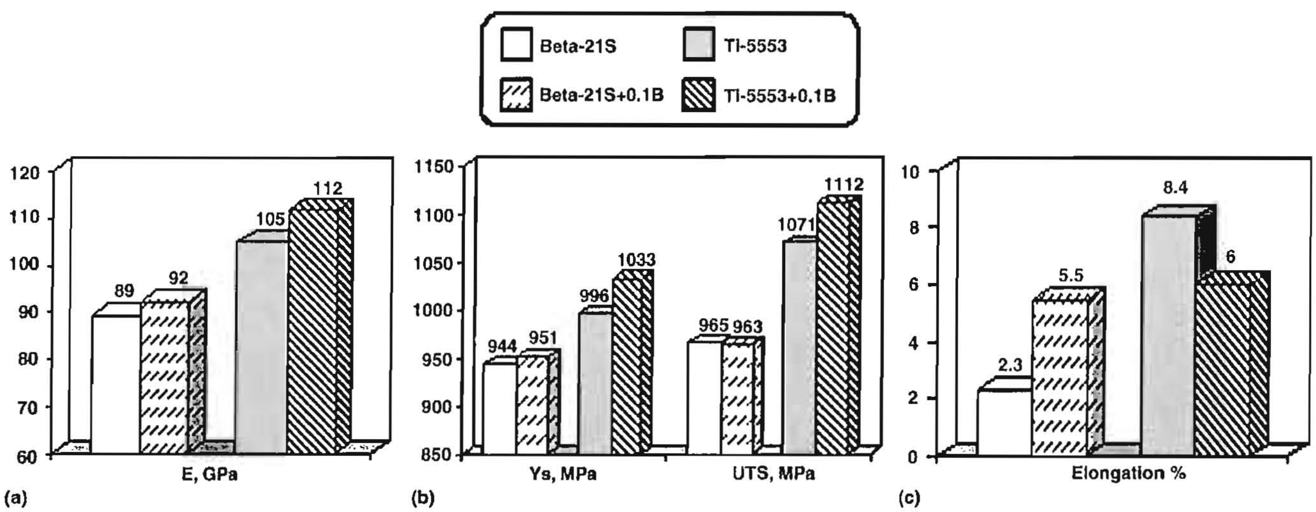

Fig. 6 Room temperature tensile properties of Beta-21S and Ti-5553 alloys containing 0 and 0.1 B: (a) elastic modulus; (b) 0.2% yield strength and ultimate tensile strength; and (c) elongation

could significantly enhance the affordability of βTi alloys. Boron additions could possibly eliminate/reduce several conventional TMP steps, which further enhances affordability.

The mechanism of grain refinement due to B additions is not expected to be similar to the classic inoculation effect observed in Al alloys (Ref 9), because the TiB phase precipitates after the β phase during solidification under equilibrium conditions for B concentrations below the eutectic limit (Ref 10). Grain refinement in TiAl-based alloys by B additions was well-studied and documented (Ref 11). Although different mechanisms have been proposed previously for B-induced grain refinement in these alloys, an alternative hypothesis based on renucleation in the constitutionally supercooled zone ahead of the solidification front appears to correlate well with the ex-

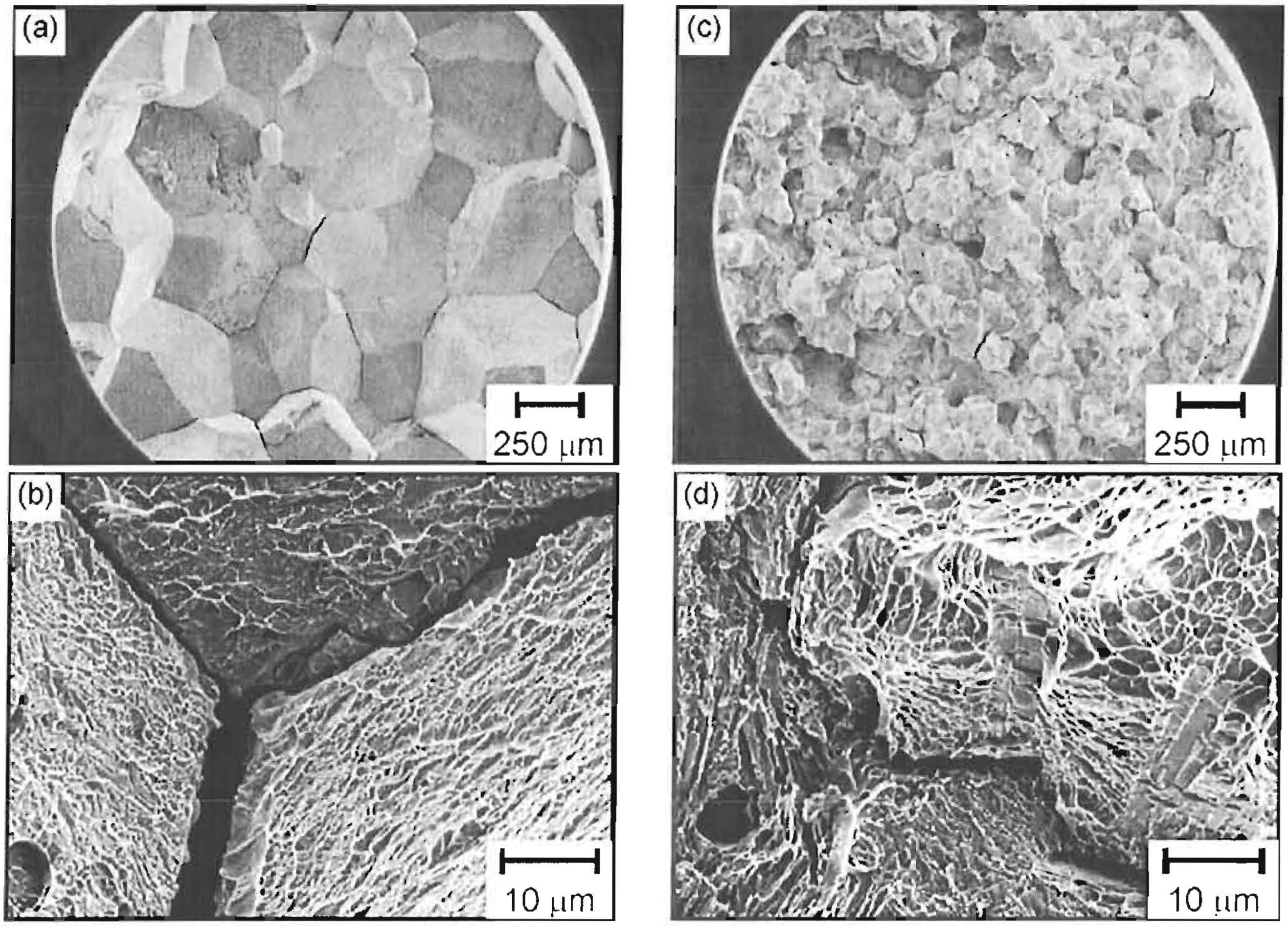

Fig. 7 Fractographs of (a, b) Beta-21S and (c, d) Beta-21S – 0.1B tensile fracture surfaces

perimental observations (Ref 12). A similar mechanism could be expected in the conventional Ti alloys (Ref 13). The preferential segregation of TiB to the grain boundaries could reduce grain growth at high temperatures via Zener pinning. More work is underway to understand the mechanism of grain refinement and to correlate with microstructural observations.

3.2 Tensile Properties

The tensile properties at room temperature of all of the β alloys considered in this study are shown in Fig. 6. The addition of 0.1 B increases the elastic modulus and strength by about ~5% while retaining good ductility. Both the fine grain size (Hall-Petch strengthening) and TiB (load-sharing mechanism) are expected to contribute to the strengthening in the B-modified alloys. A modeling effort is underway to quantify the contribution of each mechanism.

The ductility of the Beta-21S alloy in the cast condition is very low, but the B addition significantly enhanced the elongation (Fig. 6c). To understand the damage mechanism, the fracture surfaces were observed with SEM. Fractographs of the Beta-21S alloys are presented in Fig. 7. Intergranular fracture was observed in both of the alloys. However, the fracture path was straight due to the continuous grain boundary α in the Beta-21S alloy (Fig. 7b), whereas a more tortuous fracture path was observed in the Beta-21S-0.1B alloy (Fig. 7d), which explains the enhanced ductility.

The tensile strengths of the Ti-5553 and Ti-5553-0.1B alloys at elevated temperatures up to 400 °C are shown in Fig. 8. These plots show that the strength enhancements resulting from B addition observed at room temperature (Fig. 6b) are maintained at elevated temperatures. Higher strength at elevated temperature due to B additions could lead to the enhanced elevated temperature capability of these alloys, which further enhances the affordability of βTi alloys.

4. Conclusions

Two metastable βTi alloys (Beta-21S and Ti-5553) that were microalloyed (0.1%) with B were produced using conventional melt processing. The influence of B on the microstructures and tensile properties in the cast + HIP condition was established. The following conclusions are made based on the observations in this study.

- Beta Ti alloys modified with B were successfully produced using a conventional casting method.
- The addition of 0.1% B to Beta-21S and Ti-5553 alloys significantly refines the cast grain size by a factor of ~5. Micro-B additions produce a cast grain size of ~50 μm, which is typically obtained after thermo-mechanical processing (TMP) in the β phase field.
- Micro B additions provide a ~5% increase in strength and stiffness while maintaining good ductility.

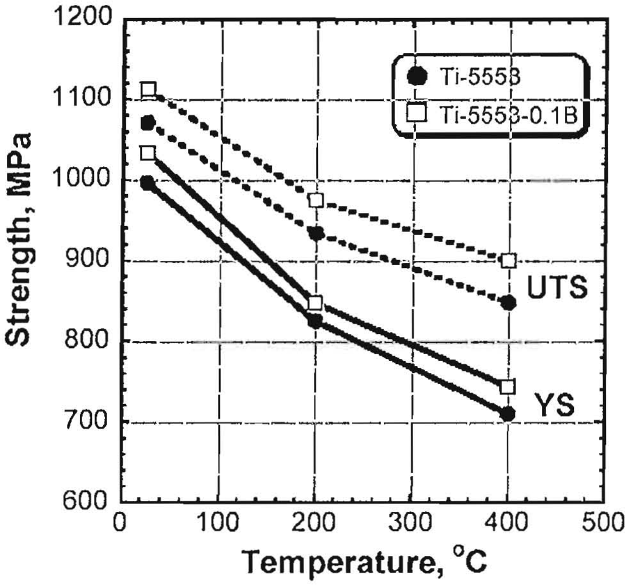

Fig. 8 Elevated temperature strengths of Ti-5553 and Ti-5553-0.1B. YS, yield strength; UTS, ultimate tensile strength

- Strength enhancements due to B additions to Ti-5553 are also maintained at elevated temperatures up to 400 °C. The ability to retain higher strength enables a better elevated temperature capability for βTi alloys.
- Micro-B additions enhance the affordability of βTi alloys via grain refinement, enhanced mechanical properties, and enhanced elevated temperature capability, and may also reduce the processing costs via the reduction/elimination of TMP steps.

Acknowledgments

This research was performed as part of the in-house research effort at the Materials and Manufacturing Directorate of the Air Force Research Laboratory. One of the authors (S.T.) is supported under the auspices of Air Force contract F33615-03-D-5801. The authors acknowledge helpful discussions with Dr. Patrick Martin and Professor M.H. Loretto.

References

1. G. Terlinde and G. Fischer, Beta Titanium Alloys, *Titanium and Titanium Alloys: Fundamentals and Applications*, C. Leyens and M. Peters, Ed., Wiley-VCH Verlag GmbH, Weinheim, 2003, p 37-57
2. P.J. Bania, Beta Titanium Alloys and Their Role in the Titanium Industry, *Beta Ti Alloys in the 1990's*, D. Eylon, R.R. Boyer, and D.A. Koss, Ed., The Materials Society, 1993, p 3-14
3. TIMET, personal communication, 2005
4. T.M. Godfrey, P.S. Goodwin, and C.M. Ward-Close, Titanium Particulate Metal Matrix Composites: Reinforcement, Production Methods, and Mechanical Properties, *Adv. Eng. Mater.*, Vol 2, 2000, p 85-92
5. Titanium-Boron: Alloys and Composites, *JOM*, Vol 56, 2004, p 32-63
6. A.E. Palty, H. Margolin, and J.P. Nielsen, Titanium-Nitrogen and Titanium-Boron Systems, *Trans. ASM*, Vol 46, 1954, p 312-328
7. S. Tamirisakandala, R.B. Bhat, D.B. Miracle, and J.S. Tiley, Microstructural Refinement in Ti Alloys Via Boron Modification, International Patent Application, filed Dec 2003
8. R.R. Boyer, E.W. Collings, and G.E. Welsch, Ed., *Materials Properties Handbook: Titanium Alloys*, ASM International, 2004
9. A. Cibula, "The Effect of Grain Size on the Tensile Properties of High Strength Cast Aluminum Alloys," 1949-1950, p 361-376
10. J.L. Marray, P.K. Liao, and K.E. Spear, *Binary Alloy Phase Diagrams*, H. Baker, Ed., ASM International, 1992, p 285
11. J.A. Christodoulou and H.M. Flower, The Role of Borides in Near-γ Titanium Aluminides, *Adv. Eng. Mater.*, Vol 2, 2000, p 631-638
12. T.T. Cheng, The Mechanism of Grain Refinement in TiAl Alloys by Boron Addition: An Alternative Hypothesis, *Intermetallics*, Vol 8, 2000, p 29-37
13. S. Tamirisakandala, R.B. Bhat, J.S. Tiley, and D.B. Miracle, Grain Refinement of Cast Titanium Alloys via Trace Boron Addition, *Scripts Mater.*, Vol 53, 2005, p 1421-1426

Available online at www.sciencedirect.com
SCIENCE DIRECT
ELSEVIER
Scripta Materialia 55 (2006) 63–68
Scripta MATERIALIA
www.actamat-journals.com

Viewpoint Paper

Reconstruction of three-dimensional microstructures of TiB phase in a powder metallurgy titanium alloy using montage serial sectioning

S.I. Lieberman,[a] A.M. Gokhale[a,*] and S. Tamirisakandala[b]

[a]*School of Materials Science and Engineering, Georgia Institute of Technology, Atlanta, GA 30332, United States*
[b]*Department of Mechanical Engineering, Ohio University, Athens, OH 45701, United States*

Received 31 October 2005; revised 18 November 2005; accepted 20 December 2005
Available online 30 January 2006

Abstract—Three-dimensional (3D) microstructures of TiB phase in a powder metallurgy Ti–6Al–4V–1.7B alloy processed using two different routes are reconstructed from large-area high-resolution montage serial sections. Visualizations of the 3D microstructures are used to determine the effects of the processing route on the morphology, anisotropy, and spatial distributions of TiB particles.

Keywords: Titanium alloys; Three-dimensional microstructure; Serial sectioning

1. Introduction

The addition of boron to titanium alloys such as Ti–6Al–4V can significantly enhance their strength and stiffness, along with providing good fracture resistance, as compared to boron-free alloys. These improvements are attributed to the TiB phase that precipitates in situ during processing. A eutectic reaction exists between titanium and boron, with a eutectic point at approximately 2 wt.% in the Ti–B binary system [1], and at approximately 1.56 wt.% in the Ti–6Al–4V–B quaternary system [2]. Depending on the boron concentration, two types of TiB can precipitate: coarse primary TiB at hypereutectic compositions (B > 1.56 wt.%), and fine eutectic TiB via the reaction, liquid → β^{Ti} + TiB. The morphology of primary TiB particles has been described as equiaxed clusters [3] and that of eutectic TiB as fine whiskers having roughly hexagonal cross sections [4]. Nonetheless, because they form in situ, there are no direct observations of three-dimensional (3D) morphologies and spatial distributions of TiB. Boron-modified titanium alloys can be made using a variety of techniques including conventional casting and powder metallurgy processes. These alloys can also be subjected to conventional thermomechanical processing operations such as forging, extrusion, and rolling to produce desired shapes with tailored microstructures. The wide range of compositions and processing methods available for Ti–B materials requires a thorough understanding of the relationships between the processing, microstructure, and properties, particularly how changes to one aspect will affect the others. Information from two-dimensional (2D) microstructural characterization would be inadequate for this purpose due to the complexity of the microstructures in these materials. The 3D representation and quantification of the microstructure would also be useful for the characterization, modeling, and simulation of these processing–microstructure–property relationships.

Depending on the composition, processing, and microstructural length scales of interest, a 3D microstructure can be rendered using several techniques, including X-ray computed tomography, magnetic resonance imaging (MRI), and serial sectioning. The montage serial sectioning technique is particularly suitable for microstructures that contain particles or features with significantly different length scales and with small interparticle spaces, which require the reconstruction of a large volume of 3D microstructure at a high resolution. These large 3D microstructural volume segments are also suitable to be representative volume elements

* Corresponding author. Tel.: +1 404 894 2887; fax: +1 404 894 9140; e-mail: arun.gokhale@mse.gatech.edu

1359-6462/$ - see front matter © 2006 Acta Materialia Inc. Published by Elsevier Ltd. All rights reserved.
doi:10.1016/j.scriptamat.2005.12.044

(RVEs) in finite element based simulations to predict the mechanical response of the material.

The classical serial sectioning technique, which enables the reconstruction of a small volume segment of 3D microstructure, was developed in the 1970s [5]. This technique has been used in numerous investigations to study 3D microstructures of opaque materials [6–10]. An efficient montage-based serial sectioning technique is also available [11–17] that permits the generation of a significantly large volume (~few mm^3) of 3D microstructure at a high resolution (~1 μm). For approximately the same metallographic effort, montage-based serial sectioning yields a microstructural volume containing a large number of features (such as pores, grains, or particles), which can provide a sufficiently large statistical sample for the study of topological aspects of microstructure such as feature connectivity. Recently, montage serial sectioning has been implemented in a completely automated serial sectioning set-up that utilizes a robotic arm to move the specimen back and forth between the metallographic equipment (polishing, etching, etc.), and an optical microscope to generate the montage serial sections [17].

In this contribution, a montage serial sectioning technique is applied for the reconstruction and visualization of TiB particles in a boron-modified Ti–6Al–4V alloy subjected to two different processing routes. Visualizations of the 3D microstructures are used to observe the effects of processing parameters on the morphology, anisotropy, and spatial distribution of TiB particles.

2. Experimental

2.1. Program materials

In this study, Ti–6Al–4V–1.7B produced via a pre-alloyed powder metallurgy approach at Crucible Research Corporation, Pittsburgh, PA, is investigated. In this process, the liquid melt of Ti–6Al–4V containing boron was rapidly solidified using inert gas atomization to produce Ti–6Al–4V–1.7B powder. The Ti–6Al–4V–1.7B powder of 100 mesh size (average particle size of 50 μm), was packed inside a thick-walled can of Ti–6Al–4V, vacuum outgassed at 300 °C for 24 h, and sealed. The can was heated to 1200 °C, soaked for 1 h, and then blind-die compacted in an extrusion chamber heated to 260 °C. The billet height was reduced by about 30% at a ram speed of 6.35 mm s^{-1}, and the compact was held at a pressure of 1400 MPa for 180 s and subsequently air-cooled to room temperature. A second billet blind die compacted by the same method was subsequently hot extruded at 1100 °C with an extrusion ratio of 16.5:1, at a ram speed of 6.35 mm s^{-1}, and air-cooled to room temperature. The selected composition lies in the hyper-eutectic regime, and the microstructures after processing consisted of coarse primary TiB as well as eutectic TiB. More information on the processing and 2D characterization of these alloys can be found elsewhere [18]. Specimens were sectioned from the compacted billet and extruded rod, and were prepared for metallographic observations using standard grinding and polishing techniques to obtain a final surface finish of 0.05 μm.

2.2. Montage serial sectioning

To generate a large volume of 3D microstructure at high resolution, one may first reconstruct a small microstructural volume such as the one in Figure 1a, and then reconstruct many contiguous small volumes surrounding it, perfectly match their boundaries, and paste them together to generate a large microstructural volume, as shown in Figure 1b. A technique equivalent to such a reconstruction has been developed [11,15,16], and is applied in this contribution for the reconstruction of 3D TiB distributions. First, a "montage" of a large number of contiguous microstructural fields (225 fields in the present case), is constructed where each microstructural field of view is grabbed at a high magnification (800× for the present microstructure). The basic principle for large-area high-resolution montage construction is described in detail by Louis, Gokhale, and co-workers [12,19,20].

In the present work, the montages were created using the automated AxioVision digital image analysis system from Carl Zeiss, Inc., that utilizes the image cross correlation function based technique for matching the borders between contiguous microstructural fields. In the present case, each montage is a microstructural image of a large area (~1.76 mm^2), having a high resolution (~0.5 μm). Figure 2a shows one such montage of 195 fields of view (FOV), which has been compressed for display. Each region of this montage has the high resolution of the images shown in Figure 2b and c. Once the montage of the first serial section is created and stored in the computer memory, a small thickness of the specimen is removed by polishing (approximately 1 μm in the present case), and then a second montage is created at the region exactly below that in the first metallographic plane. In the present study, this polish–montage–polish procedure was repeated to obtain a stack of 75 montage serial sections.

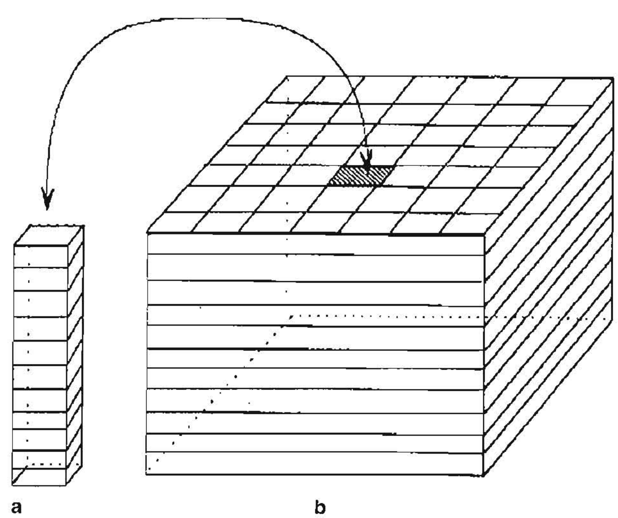

Figure 1. (a) Small microstructural volume element constructed from a stack consisting of one field of view in each serial section. (b) Large volume of microstructure obtained from contiguous small volumes such as those in (a) by using montage serial sectioning [11].

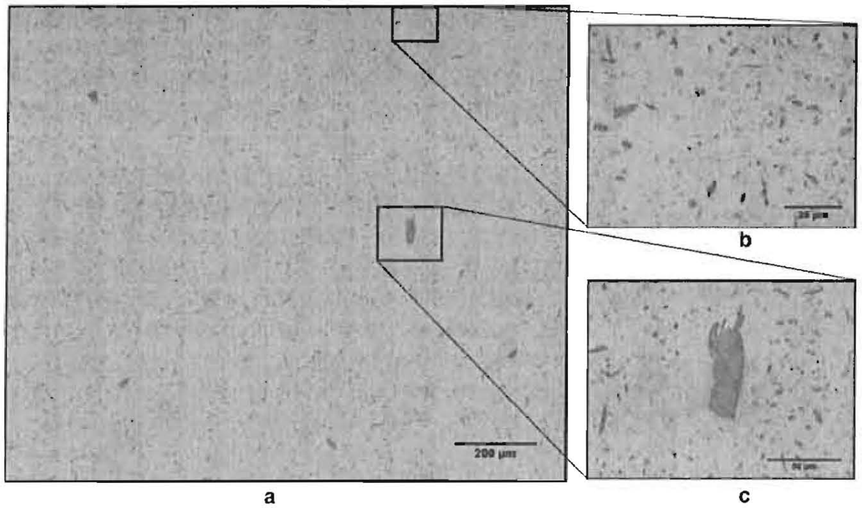

Figure 2. (a) Montage of 195 fields of view covering an area of 1.5 mm^2 created by matching contiguous microstructural fields captured at a resolution of approximately 0.5 μm. The montage is digitally compressed for presentation. Each field of view in the montage has been captured at the resolution of the images shown in (b) and (c). (b) Field of view showing eutectic TiB whiskers. (c) Field of view showing both eutectic TiB whiskers and a coarse primary TiB particle.

Microhardness indents were used to locate the exact region of interest in successive serial sections and also to precisely measure the distance between consecutive serial sections [11,13]. An important practical problem in the reconstruction of a 3D microstructure from serial sections is that the successive serial sections may not be precisely aligned; they may have some translational and rotational displacement with respect to each other. In the present study, due to slight sample adjustment on the microscope stage, the montages of consecutive serial sections were often displaced by approximately ±10 pixels and ±5 degrees, and therefore, it was essential to precisely align successive serial sections. Alignment can be achieved by locating two common points (the microhardness indents were used for this purpose), in two consecutive serial sections and translating one image until the first common point is aligned in the two images. Then the image is rotated about this point until the second common point is also aligned. In the present case, this was accomplished using the image analysis software KS 400 from Carl Zeiss, Inc., in which the images of the montage were digitally translated and rotated until they were exactly aligned with the respective previous sections.

2.3. Reconstruction and visualization of 3D microstructures

The stack of aligned serial sections essentially constitutes a volume image data set similar to those encountered in X-ray computed tomography and MRI. Therefore, the same three-dimensional microstructure visualization techniques are applicable. The 3D microstructure visualization can be achieved either by volume rendering or by surface rendering. Volume rendered images can be used as RVEs for finite element based computations [21]. Surface rendering involves the rendering of the iso-surface of the region of interest (ROI) from the volume data, whereas volume rendering is the rendering of all volume data by specifying opacity and color of each voxel (3D pixel). Surface rendering leads to a reduction in the size of the data set because only the surface data are retained. Surface rendering requires the fitting of a surface in the volume data. Numerous algorithms are available for surface rendering, including the contour connecting algorithm [22] and the marching cube algorithm [23]. In the present work, the marching cube algorithm was employed for the surface rendering of the 3D microstructures, using the image analysis software VayTek VoxBlast 3.10. The effective resolution of the 3D microstructures is approximately 1 μm, which is the depth of material removed between serial sections. Measurements on the 3D rendered images were performed using the image analysis software Image-Pro Plus 3D Suite 5.1 from Media Cybernetics, Inc.

3. Results and discussion

In the present work, the 3D microstructure visualization was completed using 75 montage serial sections, with each montage serial section containing 225 contiguous microstructural fields grabbed at a magnification of 800×. Therefore, the resulting 3D data sets are useful for the characterization and visualization of the microstructure at fine as well as at coarse length scales. Figure 3a shows a stack of 20 aligned montage serial sections of the microstructure of extruded Ti–6Al–4V–1.7B having aligned eutectic TiB whiskers. The extrusion direction is perpendicular to the plane of the serial sections in this micrograph. Figure 3a shows 16 contiguous fields of view cropped from serial sections of 225 contiguous microstructural fields (this figure has been digitally compressed for presentation). Figure 3b is the magnified view of the outlined region in Figure 3a, where each section is exactly the stack of serial sections generated by the single field of view type classical serial sectioning

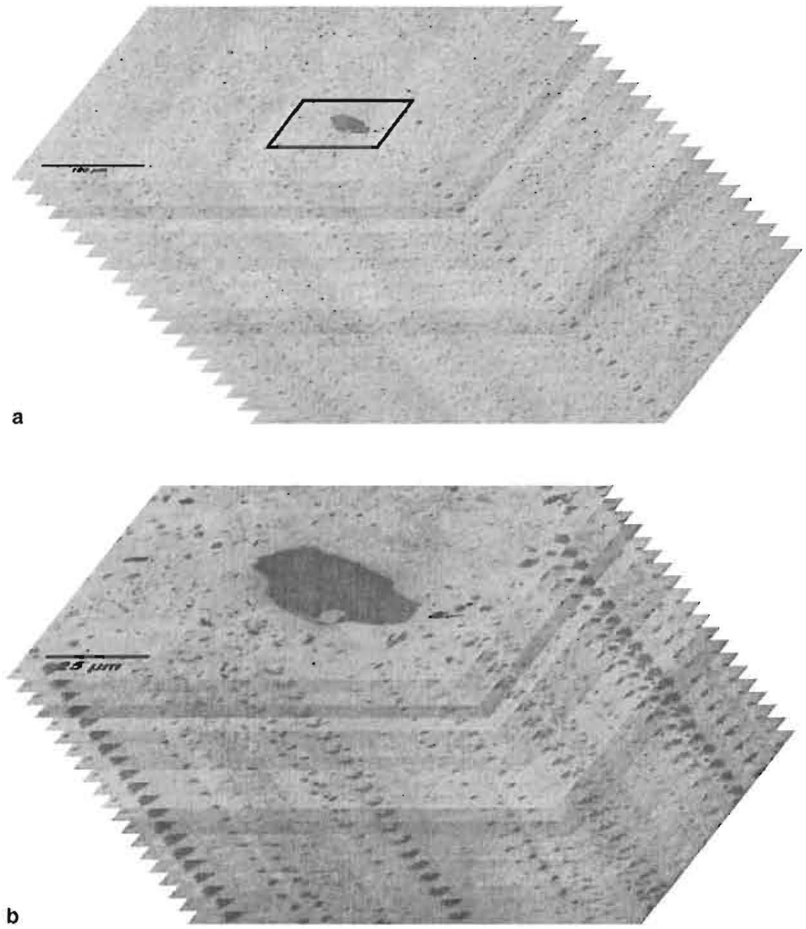

Figure 3. (a) Stack of 20 montage serial sections for the extruded Ti–6Al–4V–1.7B microstructure. Each serial section in this figure contains 16 contiguous microstructural fields. (b) The magnified view of the outlined region of the stack of 20 montage serial sections in (a). This is the resolution of the individual microstructural fields.

technique [5–10]. This is the magnification at which all microstructural fields of the montages have been grabbed. In Figure 3b, changes in the sizes of the whiskers at the edges of these serial sections as well as the appearance and disappearance of features in successive serial sections can be observed.

Figure 4 shows a segment of the surface rendered 3D microstructure of the extruded alloy depicting the spatial distribution of anisotropic eutectic TiB whiskers. This segment also contains a coarse primary TiB particle in the center of the image that is approximately an order of magnitude larger than the eutectic TiB whiskers. In this rendering, images were digitally segmented to completely remove the matrix and reveal only TiB. Note that this volume segment is only about 0.5% of the total microstructure volume collected from the stack of 75 montage serial sections (to produce the 3D rendering at the resolution of the eutectic TiB whiskers). Figure 4 clearly shows that the eutectic TiB whiskers have anisotropic orientations after extrusion and that the majority of them are aligned along the extrusion direction, which is the z-axis of the box.

Figure 5 shows a volume segment of the surface rendered 3D microstructure of the as-compacted alloy containing only eutectic TiB whiskers. Figure 6 shows another volume segment of the surface rendered 3D microstructure of the as-compacted alloy that contains both a coarse primary TiB particle and eutectic TiB whiskers. Observe that the TiB whiskers in this microstructure have uniform random angular orientations, as opposed to the anisotropic orientations in the compacted and extruded alloy microstructure (Fig. 4). Therefore, it can be concluded that plastic deformation during the extrusion process gives rise to rigid body rotations of the TiB whiskers, which confirms the conclusion reached by Schuh and Dunand [24] on the basis of 2D microstructural observations. Although the morphological orientation distribution of the eutectic TiB whiskers is different in the compacted microstructure as compared to the extruded microstructure, the spatial arrangement of the eutectic TiB whiskers appears to be uniform random in both of the 3D microstructures. Therefore, although the extrusion process leads to TiB whisker rotations, it does not give rise to spatial clustering of the whiskers.

Figure 7a shows various 3D views of just the primary TiB particle extracted from Figure 4. This primary TiB particle is present in each of the 75 serial sections of the extruded alloy, and it is truncated by the first and the last serial sections. The part of the volume of this

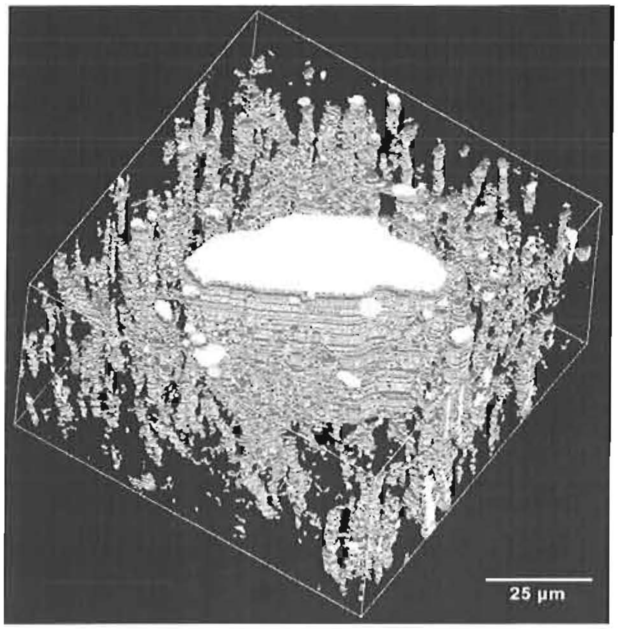

Figure 4. Small segment of surface rendered 3D microstructure of extruded Ti–6Al–4V–1.7B, showing the eutectic TiB whiskers around a coarse primary TiB particle. This 3D microstructure shows the alignment of the majority of the eutectic TiB whiskers along the extrusion direction (which is the z-axis in this figure).

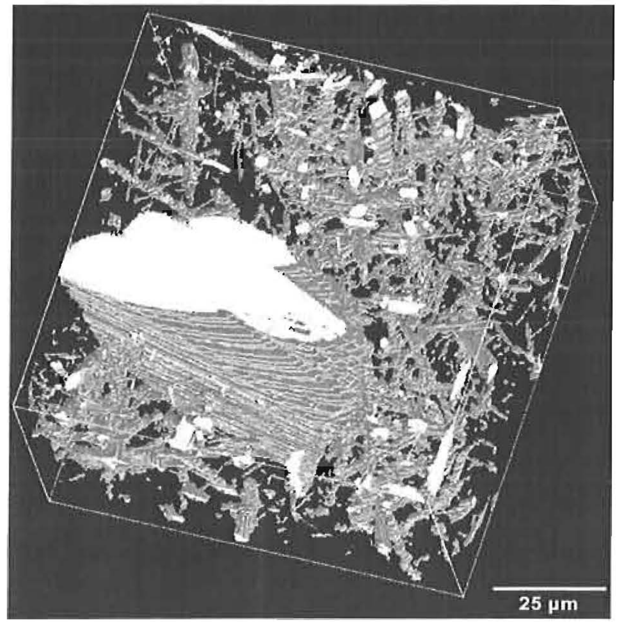

Figure 6. Small segment of surface rendered 3D microstructure of as-compacted Ti–6Al–4V–1.7B, showing both the eutectic TiB whiskers and a coarse primary TiB particle.

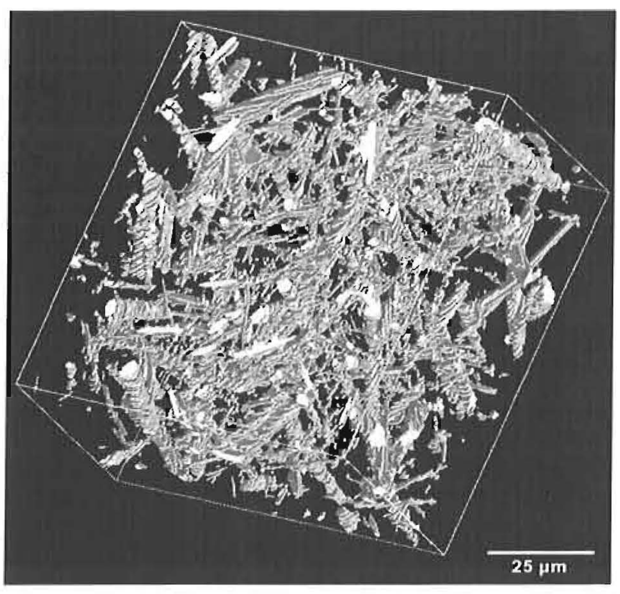

Figure 5. Small segment of surface rendered 3D microstructure of as-compacted Ti–6Al–4V–1.7B revealing uniform random angular orientations of the eutectic TiB whiskers.

particle contained between the first and the last serial sections is 67,000 μm^3, the surface area is 12,300 μm^2, and the axial ratio is 3.76, which provide a lower bound on the true volume, surface area, and axial ratio of the particle. Therefore, the primary TiB particle has an elongated shape rather than an equiaxed shape as reported in the literature [3]. Detailed 3D quantitative microstructural data obtained from these reconstructed 3D images will be presented in another contribution.

Figure 7b shows various 3D views of a eutectic TiB whisker extracted from the volume segment of the surface rendered 3D microstructure of the as-compacted alloy in Figure 5. This eutectic TiB whisker is approximately an order of magnitude smaller in size than a primary TiB particle. While the surface rendered primary TiB particles have been truncated by the boundaries of the 75 serial sections, the eutectic TiB whisker in Figure 7b is whole.

Figure 7c shows various 3D views of the coarse primary TiB particle extracted from the 3D microstructure of the as-compacted alloy in Figure 6. The morphology (elongated shape), and the length scale of the primary TiB particle in the as-compacted alloy (Fig. 7c) are very similar to that in the extruded alloy (Fig. 7a). The primary TiB particle shown in Figures 6 and 7c is present in 65 of the serial sections, and it is truncated by the last serial section. The part of the volume of this particle contained between the first and the last serial sections is 53,400 μm^3, the surface area is 11,600 μm^2, and the axial ratio is 3.29, which is a lower bound on the true volume, surface area, and axial ratio of the particle.

4. Summary and conclusions

A montage serial sectioning technique has been used to generate high resolution (~0.5 μm), large-volume (0.13 mm^3), 3D microstructures of a powder metallurgy Ti–6Al–4V–1.7B alloy containing TiB whiskers/particles in two different process conditions (compacted and extruded). The visualization of the reconstructed 3D microstructures provides important insights on the 3D morphologies and spatial distribution of coarse primary

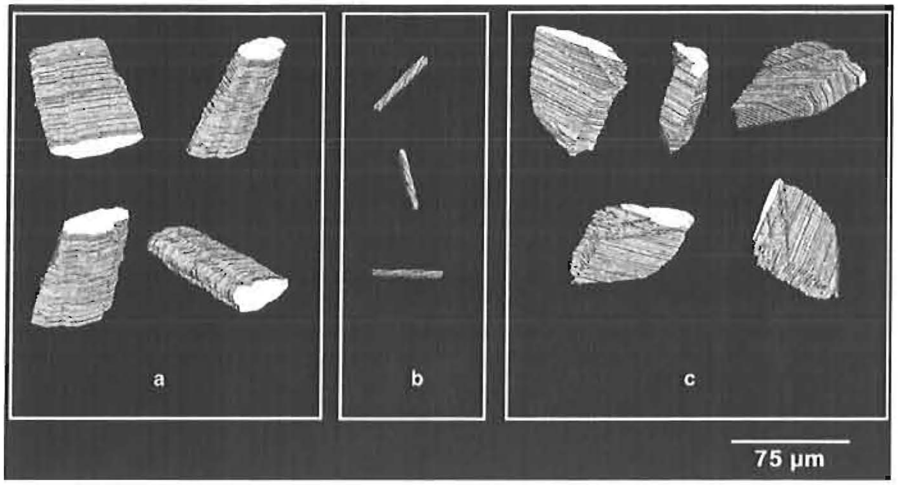

Figure 7. (a) 3D views of the primary TiB particle extracted from the surface rendered 3D microstructure of the extruded Ti–6Al–4V–1.7B sample shown in Figure 4. (b) 3D views of a eutectic TiB whisker extracted from the surface rendered 3D microstructure of as-compacted Ti–6Al–4V–1.7B shown in Figure 5. (c) 3D views of the primary TiB particle extracted from the surface rendered 3D microstructure of as-compacted Ti–6Al–4V–1.7B shown in Figure 6.

TiB particles as well as of fine eutectic TiB whiskers. Both of these phases possess elongated morphology, although the primary TiB size is approximately an order of magnitude larger than that of eutectic TiB. In the as-compacted condition, the eutectic TiB whiskers have uniform random angular orientations, whereas after extrusion they tend to be aligned along the extrusion direction via rigid body rotation.

Acknowledgement

This research is supported through research grants from the Air Force Office of Scientific Research (AFOSR grant number F49620-01-1-0045). Dr. J.S. Tiley is the AFOSR Program Manager for this grant. The financial support is gratefully acknowledged. The authors acknowledge helpful discussions with Dr. D.B. Miracle of the Air Force Research Laboratory. Any opinions, findings, and conclusions or recommendations expressed in this contribution are those of the authors and do not necessarily reflect the views of the funding agencies.

References

[1] J.L. Murray, P.K. Liao, K.E. Spear, in: H. Baker (Ed.), Binary Alloy Phase Diagrams, ASM International, Materials Park, OH, 1992, p. 285.
[2] O.M. Ivasishin, Institute for Metal Physics, Ukraine, private communication, 2005.
[3] Z. Peng, S.B. Bhaduri, G.L. Watt, in: K.V. Logan, Z.A. Munir, R.M. Spriggs (Eds.), Advanced Synthesis and Processing of Composites and Advanced Ceramics II, American Ceramic Society, Westerville, OH, 1996, p. 11.
[4] T. Saito, J. Metals (2004) 33.
[5] F.N. Rhines, K.R. Craig, Metall. Trans. A 7A (1976) 1729.
[6] R.S. Sidhu, N. Chawla, Mater. Charact. 52 (2004) 225.
[7] M. Li, S. Ghosh, O. Richmond, H. Weiland, T.N. Rouns, Mater. Sci. Eng. A265 (1999) 153.
[8] K.M. Wu, M. Enomoto, Scripta Mater. 46 (2002) 569.
[9] M.V. Kral, M.A. Mangan, G. Spanos, R.O. Rosenberg, Mater. Charact. 45 (2000) 17.
[10] T. Yokomizo, M. Enomoto, G. Spanos, R.O. Rosenberg, Mater. Sci. Eng. 344A (2003) 261.
[11] A. Tewari, A.M. Gokhale, R.M. German, Acta Mater. 47 (1999) 3721.
[12] A.M. Gokhale, A. Tewari, J. Microsc. 200 (2000) 277.
[13] A. Tewari, A.M. Gokhale, Mater. Charact. 46 (2001) 329.
[14] M.D. Dighe, A. Tewari, G.R. Patel, T. Mirabelli, A.M. Gokhale, Trans. Am. Foundry Soc. 99 (2000) 353.
[15] A. Tewari, Ph.D. Dissertation, Georgia Institute of Technology, 1999.
[16] H. Singh, A.M. Gokhale, Mater. Charact. 54 (2005) 21.
[17] J.E. Spowart, H.M. Mullens, B.T. Puchala, J. Metals (2003) 35.
[18] S. Tamirisakandala et al., Scripta Mater. 53 (2005) 217.
[19] P. Louis, A.M. Gokhale, Metall. Mater. Trans. A 26A (1995) 1449.
[20] P. Louis, A.M. Gokhale, Acta Mater. 44 (1996) 1519.
[21] P. Sabella, Comp. Graphics 22 (1988) 51.
[22] E. Keppel, IBM J. Res. Devel. 19 (1975) 2.
[23] E.W. Lorensen, H.E. Cline, Comp. Graphics 22 (1987) 38.
[24] C. Schuh, D.C. Dunand, Int. J. Plast. 17 (2001) 317.

ELSEVIER

Available online at www.sciencedirect.com

SCIENCE DIRECT

Scripta Materialia 55 (2006) 465–468

Scripta MATERIALIA

www.actamat-journals.com

In situ scanning electron microscopy observations of tensile deformation in a boron-modified Ti–6Al–4V alloy

C.J. Boehlert,[a,*] C.J. Cowen,[a] S. Tamirisakandala,[b] D.J. McEldowney[c] and D.B. Miracle[d]

[a] *Department of Chemical Engineering and Materials Science, Michigan State University, 2527 Engineering Building, East Lansing, MI 48824-1226, United States*

[b] *Department of Mechanical Engineering, Ohio University, Athens, OH 45701, United States*

[c] *Department of Chemical and Materials Engineering, University of Dayton, Dayton, OH 45469, United States*

[d] *Air Force Research Laboratory, Materials and Manufacturing Directorate, Wright-Patterson AFB, OH 45433, United States*

Received 22 February 2006; revised 28 April 2006; accepted 9 May 2006
Available online 9 June 2006

In situ scanning electron microscopy was performed during both room temperature and 480 °C tensile deformation of a boron-modified Ti–6Al-4V alloy, in order to characterize the deformation evolution. The sequence of observable surface deformation events was: TiB whisker microcracking at stresses well below the global yield stress, multiple and extensive TiB cracking after global yielding, $\alpha + \beta$ phase slip emanating from the cracked TiB whiskers, localized shear band formation and propagation leading to cracking in the $\alpha + \beta$ phases, and ductile sample failure. TiB cracking was also observed throughout the subsurface locations on post-deformed samples. The early microcracking of TiB particles did not degrade mechanical properties, and higher tensile and ultimate strengths were obtained with a ductile fracture mode at quasi-static tensile elongations equivalent to conventional Ti-6Al-4V.

Keywords: Titanium alloys; SEM; Tension test; Fracture

Conventional titanium (Ti) alloys containing small additions of boron (B), henceforth termed Ti–B alloys, have been attracting considerable interest in recent years due to their mechanical properties, which include high specific stiffness and strength along with reasonable elongation-to-failure (ε_f) [1–24]. The typical room temperature (RT) Young's modulus, yield strength, and ultimate strength values for Ti-6Al-4V(wt.%)[1] are 110 GPa, 986 MPa, and 1035 MPa, respectively [9], while for the following B-modified alloys the associated measured values are: Ti–6Al–4V–0.9B: 127 GPa, 1190 MPa, and 1312 MPa; Ti–6Al–4V–1.7B: 136 GPa, 1202 MPa, and 1359 MPa; Ti–6Al–4V–2.2B: 144 GPa, 1315 MPa, and 1470 MPa [2]. The significant increase in strength and stiffness in Ti–B alloys arise from the strong and stiff TiB whiskers ($E \sim$371–482 GPa) that precipitate *in situ* due to B additions [3,23]. In addition, significant grain refinement is also achieved due to B addition, which leads to further strengthening [7]. TiB has essentially the same density as Ti alloys, so that the higher strength and stiffness of Ti–B alloys provides important increases in specific strength and stiffness. The aforementioned studies on Ti–B alloys show that dramatic microstructural and mechanical property alterations are possible through relatively small B additions. Although Ti–B alloys are currently used for various commercial applications (e.g. exhaust valves of automotive engines) [1], understanding the micromechanisms of deformation and fracture is necessary to consider these materials for fracture-critical applications (e.g. aerospace). This would also help in optimizing processing–microstructure–property relationships. In this paper, we use an *in situ* technique of surface imaging during tensile testing to gain an understanding of the deformation evolution in Ti–B alloys.

Pre-alloyed powder with a nominal composition of Ti–6Al–4V–1B, produced via inert gas atomization (Crucible Research Corporation, Pittsburgh, PA), was used in this study. One kg of powder was packed inside a thick-walled Ti–6Al–4V can of 70 mm diameter and 130 mm length, vacuum outgassed at 300 °C for 24 h, and sealed. The can was heated to 1200 °C, soaked for 1 h, and compacted in an extrusion chamber using a

* Corresponding author. Tel.: +1 517 353 3703; fax: +1 517 432 1105; e-mail: boehlert@egr.msu.edu

[1] All alloy compositions are given in weight percent.

1359-6462/$ - see front matter © 2006 Acta Materialia Inc. Published by Elsevier Ltd. All rights reserved.
doi:10.1016/j.scriptamat.2006.05.008

blind-die. The compact was held at a pressure of 1400 MPa for 180 s followed by air-cooling to RT. A length reduction of approximately 30% occurred during compaction, and full density was achieved. The compact was then extruded at 1100 °C through a conical die using a 16:1 extrusion ratio. The chemical composition of the extruded product in weight per cent was measured to be Al-6.5, V-3.61, B-1.06, O-0.125, Fe-0.036, H-0.01, C-0.1, N-0.01, and Ti-Balance. Metallographic samples were sectioned, ground, and polished to expose the microstructures. Microstructural observations were made on unetched specimens using a field-emission, high-resolution scanning electron microscope (SEM) in the backscattered electron (BSE) imaging mode.

Flat dog-bone-shaped samples, with gage portion dimensions of 3 mm wide × 2.5 mm thick × 10 mm long (Fig. 1), were machined from the extruded rod via electric discharge machining, with the tensile axis parallel to the extrusion direction. A slight (0.6 mm) reduction in the width of the sample was introduced in a portion of the gage section to ensure that the failure occurred at this location, and therefore the *in situ* deformation and fracture features could be captured in the SEM observations. To remove the recast layer and to provide a suitable surface for observation, the specimens were glued to a metallic platen and polished through a 0.06 μm finish using an automatic polishing machine. Tensile tests were performed at RT and 480 °C using a screw-driven tensile stage (Ernest F. Fullam, Inc., Lantham, NY) placed inside the SEM chamber (Fig. 2). The *in situ* load–displacement relationship was obtained during experiments using MTESTW version F 8.8e data acquisition and control software (Admet, Inc., Norwood, MA) which allowed for either load or displacement control testing. Four RT experiments were performed in either an FEI XL-30 or CAMSCAN44FE SEM chamber. The experiments were performed using either load control at 3.7 or 7.3 N/s loading rates, or displacement control at a rate of 25 μm/s. One test was conducted at 480 °C with a tungsten-based heating element, using a power supply in constant voltage mode, placed just below the gage section of the sample. Oxidation did not affect the *in situ* imaging characterization as the pressure within the SEM chamber never exceeded 10^{-6} Torr. At certain load levels, both below and above the elastic limit, the experiments were paused and SEM imaging was performed. The imaging process took between 60 and 180 s and a slight load relaxation occurred during the pauses. After imaging, the load or displacement rate was continued at the same level. The displacement data acquired during the experiments comprised that of the sample as well as the gripping fixtures. Efforts are underway to test the samples with strain gages attached, which will facilitate measurement of the sample's displacement exclusively.

Conventional tensile tests were also conducted using round threaded specimens of 3 mm gage diameter and 20 mm gage length. A constant crosshead speed of 0.01 mm s^{-1} was used and the displacement in the gage portion was recorded using a 10 mm gage length extensometer attached to the specimen.

As verified with X-ray diffraction and microstructural analysis, the alloy contained TiB whiskers mixed with the $\alpha + \beta$ two-phase microstructure typical for a Ti–6Al–4V alloy. The microstructures along the longitudinal and transverse directions are shown in Figure 3. In these and subsequent micrographs, TiB is the dark phase, the light phase is β, and the gray phase is α. TiB was in the form of short whiskers aligned along the extrusion direction (Fig. 3a) and exhibited roughly hexagonal cross-sections (Fig. 3b). The lengths of the TiB whiskers ranged from a few microns to 30 μm. The average diameter of the TiB whiskers was 3.2 μm ± 1.2 μm and they occupied a volume of 7.3% ± 1.5%.

A typical stress–displacement curve at RT is shown in Figure 4. Various stress levels at which the test was paused for SEM imaging are marked on this plot. Figure 5(a–j) illustrate images taken at sequential load levels during the RT deformation. The alloy exhibited global yielding above 1050 MPa and surface microcracks in the TiB whiskers were observed at stresses well below the global yield stress (Fig. 5b). The microcracks grew and became more extensive in the TiB whiskers (Fig. 5f–i) as the load was increased above the global yield stress. Figure 5(h) and (i) indicate that slip emanated from the cracked TiB whiskers where high stress concentrations existed. Localized shear bands formed and propagated leading to cracking in the α and β phases. A similar sequence of surface deformation events has been noted for a B-modified Ti–6Al–4V alloy containing 0.5 wt.%B during RT tensile fatigue [9], where

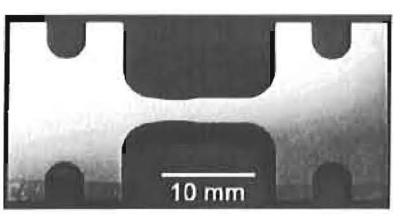

Figure 1. Photograph of the tensile specimen used for the *in situ* studies performed in the SEM.

Figure 2. Image taken inside the SEM chamber showing the tensile stage setup.

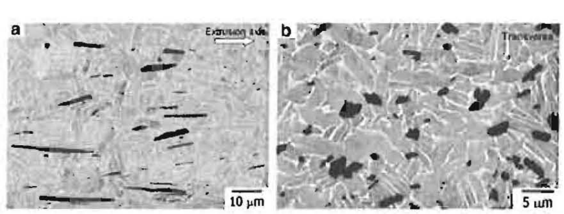

Figure 3. BSE images of the extruded Ti–64–1B microstructure in the (a) longitudinal and (b) transverse directions.

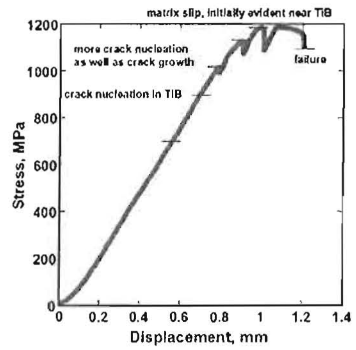

Figure 4. Tensile stress vs. displacement curve for Ti–64–1B during an RT *in situ* experiment where imaging was performed at the stress levels marked on the curve (0, 715, 925, 1018, 1129, 1187, 1172 MPa and failure).

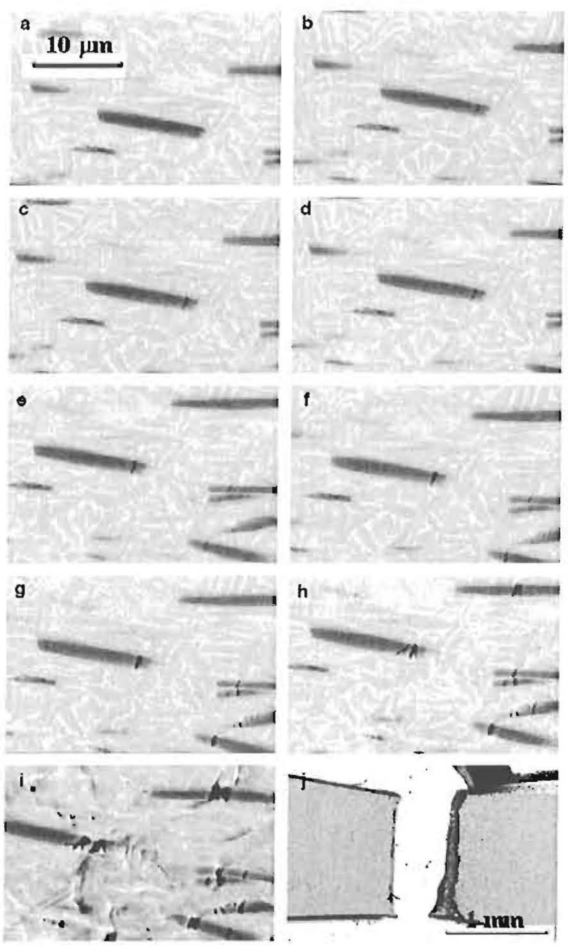

Figure 5. BSE images taken during a load-controlled RT tensile experiment at stress levels of (a) 0 MPa, (b) 829 MPa, (c) 913 MPa, (d) 956 MPa, (e) 1013 MPa, (f) 1069 MPa, (g) 1159 MPa, (h) 1187 MPa, (i) 1241 MPa, and (j) after failure.

transverse cracking in TiB whiskers and interfacial decohesion events lead to matrix crack initiation. Crack initiation at ceramic particles or whiskers and propagation into Ti–6Al–4V matrices has also been observed elsewhere [25,26]. However, the *in situ* surface observations of this work revealed that although microcracking of the TiB whiskers occurred prior to global yielding, large quasi-static tensile elongations can be accommodated in the Ti–6Al–4V–1B alloy. The large extent of matrix slip as well as dimples on the fracture surfaces (Fig. 6a and b) confirmed that the alloy tolerated a large amount of elongation before failure occurred. The above-mentioned surface deformation observations were typical for all four of the RT tensile samples tested, and a stress level of 715 MPa was the lowest stress where visible TiB whisker microcracking was evident. No *in situ* observations were made between 500 MPa and 715 MPa, thereby TiB microcracking may have occurred at stresses below 715 MPa. Features similar to those observed on the surface (multiple TiB cracking and cavitation at TiB whisker ends) were observed in the interior (Fig. 7), thereby correlating the surface observations with those for the bulk. While the quasi-static ductility is not adversely affected by early TiB failure, the response to dynamic loading needs to be studied in detail and is the topic of ongoing research.

The following tensile properties were recorded for the conventionally tensile-tested material: yield strength 1079 MPa, ultimate strength 1224 MPa, and elongation-to-failure 13%. These strength values are approximately 100 MPa below those measured by Yolton et al. [2] for a powder-processed Ti–6Al–4V–0.9B alloy that was hot isostatically pressed and extruded. The oxygen content in this alloy was 0.2%, and the measured elongation-to-failure was only 5% [2]. The oxygen content of the alloy in the current study was 0.125%. The increased strength and decreased elongation of the previously studied alloy compared to the currently studied alloy may be a result of the higher oxygen content in that material. Differences in the processing conditions, such as compaction temperature and extrusion speed, may also have played a role. Overall, the 1 wt.%B addition significantly strengthened the Ti–6Al–4V alloy without changing the

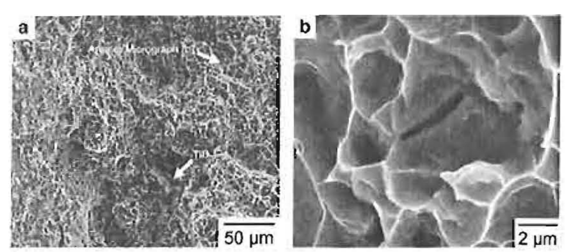

Figure 6. (a) Low- and (b) high-magnification SEM (SE) images of the fracture surface of an RT tensile tested sample where the arrow in (a) indicates the cracked TiB whisker in (b).

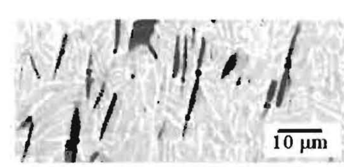

Figure 7. BSE image of the interior TiB cracking evident in the RT deformed sample in Figure 5 after failure just behind the fracture surface.

fracture mode or degrading the elongation-to-failure. The higher strengths and elastic modulus noted in this material compared to Ti–6Al–4V is a result of the strong and stiff TiB whiskers. The size, morphology, orientation, and distribution of TiB are important parameters that alter the mechanical properties of Ti–B alloys. Strength modeling on similar alloys revealed that the majority of the strength increase is attributable to the load-sharing mechanism by the TiB [27].

Figure 8 illustrates the post-yield surface deformation of the sample tested at 480 °C. This sample exhibited the same sequence of deformation events, including TiB cracking prior to global yielding, as for the samples deformed at RT. The gage section of this sample, which did not fail but was estimated to have exhibited a strain greater than 10%, was subsequently polished and imaged in the SEM to reveal subsurface deformation and cracking (Fig. 9). A significant amount of TiB cracking was observed where the interfacial void formation was noted on samples which were sectioned transverse to the loading direction.

To summarize, the tensile deformation evolution of a boron-modified Ti alloy, Ti–6Al–4V–1B, produced via a pre-alloyed powder metallurgy approach, was evaluated using surface observations during *in situ* testing in an SEM chamber. This alloy exhibited surface TiB whisker microcracking at stresses more than 300 MPa below the global yielding event. TiB cracking became more extensive after global yielding, leading to localized slip in the $\alpha + \beta$ microstructure that originated at cracked TiB whiskers. Deformation continued via large plasticity in the $\alpha + \beta$ microstructure followed by crack formation in the $\alpha + \beta$ phases before final ductile fracture. Similar deformation evolution events were observed for a sample deformed at 480 °C, and interior TiB cracking was observed similar to that noted at the sample's surface. A significant increase in the tensile yield and ultimate strength was recorded both in the *in situ* samples and in conventional tensile experiments on larger samples which were not imaged *in situ*. In spite of early failure of TiB whiskers, no debit in quasi-static tensile ductility occurred. The influence of early TiB failure under dynamic loading is not yet established and is the subject of ongoing research.

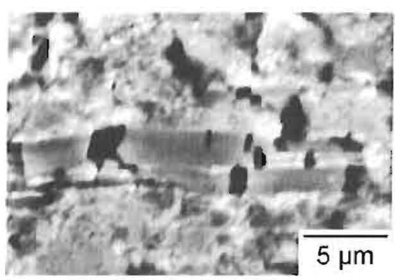

Figure 8. BSE image of the surface of a yielded sample tensile tested at 480 °C.

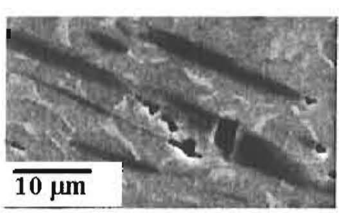

Figure 9. BSE image of the interior TiB cracking evident in the 480 °C deformed sample in Figure 8 in the extrusion direction.

This work was supported by the National Science Foundation through grants DMR-0320992 and DMR-0533954.

[1] T. Saito, JOM 56 (2004) 33.
[2] C.F. Yolton, J.H. Moll, in: P.A. Blenkinsop, W.J. Evans, H.M. Flowers (Eds.), Titanium 1995, vol. 1, Cambridge University Press, Cambridge, 1996, p. 2755.
[3] S. Gorsse, D.B. Miracle, Acta Mater. 51 (2003) 2427.
[4] T.M.T. Godfrey, A. Wisbey, P.S. Goodwin, K. Bagnall, C.M. Ward-Close, Mater. Sci. Eng. A 282 (2000) 240.
[5] S. Tamirisakandala, R.B. Bhat, V.A. Ravi, D.B. Miracle, JOM 56 (2004) 60.
[6] K.S. Ravichandran, D.B. Miracle, JOM 56 (2004) 32.
[7] S. Tamirisakandala, R.B. Bhat, J.S. Tiley, D.B. Miracle, Scripta Metall. Mater. 53 (12) (2005) 1421.
[8] S. Tamirisakandala, R.B. Bhat, D.B. Miracle, S. Boddapati, R. Bordia, R. Vanover, V.K. Vasudevan, Scripta Metall. Mater. 53 (2) (2005) 217.
[9] W.O. Soboyejo, W. Shen, T.S. Srivatsan, Mech. Mater. 36 (2004) 141.
[10] W. Lu, D. Zhang, X. Zhang, R. Wu, Scripta Metall. Mater. 44 (2001) 2449.
[11] W.O. Soboyejo, R.J. Lederich, S.M.L. Sastry, Acta Metall. Mater. 42 (1994) 2579.
[12] T.S. Srivatsan, W.O. Soboyejo, R.J. Lederich, Compos. Part A 28A (1997) 365.
[13] W. Lu, D. Zhang, X. Zhang, R. Wu, T. Sakata, H. Mori, J. Alloys Compd. 327 (2001) 240.
[14] W. Lu, D. Zhang, X. Zhang, Y. Bian, R. Wu, T. Sakata, H. Mori, J. Mater. Sci. 36 (2001) 3707.
[15] W. Lu, D. Zhang, X.N. Zhang, R.J. Wu, T. Sakata, H. Mori, Mater. Sci. Eng. A 311 (2001) 142.
[16] W.J. Lu, D. Zhang, X.N. Zhang, R.J. Wu, T. Sakata, H. Mori, Scripta Metall. Mater. 44 (2001) 1069.
[17] W.J. Lu, D. Zhang, X.N. Zhang, R.J. Wu, T. Sakata, H. Mori, Mater. Trans. JIM 41 (11) (2000) 1555.
[18] C. Schuh, D.C. Dunand, Scripta Metall. Mater. 45 (2001) 63.
[19] E. Zhang, G. Zeng, S. Zeng, Scripta Metall. Mater. 46 (2002) 811.
[20] S. Abkowitz, S.M. Abkowitz, H. Fisher, P.J. Schwartz, JOM 56 (2004) 37.
[21] K.S. Ravi Chandran, K.B. Panda, S.S. Sahay, JOM 56 (2004) 42.
[22] S. Kumari, N. Eswara Prasad, K.S. Ravi Chandran, G. Malakondaiah, JOM 56 (2004) 51.
[23] K.B. Panda, K.S. Ravi Chandran, Acta Mater. 54 (2006) 1641.
[24] D. Galvan, V. Ocelik, Y. Pei, B.J. Kooi, J.T.M. De Hosson, E. Ramous, J. Mater. Eng. Perf. 13 (2004) 406.
[25] J.A. Vreeling, V. Ocelik, J.T.M. De Hosson, Acta Mater. 50 (2002) 4913.
[26] A.B. Kloosterman, B.J. Kooi, J.T.M. De Hosson, Acta Mater. 46 (1998) 6205.
[27] Tamirisakandala S, Bhat RB, McEldowney DJ, Miracle DB. Affordable Metal Matrix Composites for High Performance Applications II, 2003, TMS, Warrendale, PA, p. 185.

ELSEVIER
Materials Characterization xx (2006) xxx–xxx
MATERIALS CHARACTERIZATION

Reconstruction of three-dimensional microstructures of TiB whiskers in powder processed Ti–6Al–4V–1B alloys

S.I. Lieberman [a], A.M. Gokhale [a,*], S. Tamirisakandala [a,b]

[a] School of Materials Science and Engineering Georgia Institute of Technology, Atlanta, GA 30332, United States
[b] Department of Mechanical Engineering, Ohio University, Athens, OH 45701, United States

Received 25 May 2006; received in revised form 26 July 2006; accepted 27 July 2006

Abstract

Visualization of three-dimensional (3D) microstructure is useful for understanding microstructural geometry. In this contribution, 3D microstructures of TiB whiskers in two powder metallurgy processed Ti–6Al–4V–1B alloys are reconstructed and visualized using large-area high-resolution montage serial sections and digital image processing to study the effects of processing route on the morphology and anisotropy of the TiB phase. The microstructures consisted of eutectic TiB in Ti-64 and are free from coarse primary phase TiB. The eutectic TiB phase has whisker morphology in both the compacted and compacted plus extruded conditions. The orientations of TiB whiskers are uniformly random in the compacted condition and highly aligned anisotropic in the extruded condition. The spatial distributions of TiB are uniform in both cases without any clustering. The large volumes of reconstructed 3D microstructures are useful for incorporation into finite element-based computations.

Keywords: Three-dimensional microstructure; Serial sectioning; Titanium alloys

1. Introduction

Additions of small amounts of boron to conventional titanium alloys increases the structural efficiency (a combination of specific strength and specific stiffness), while maintaining adequate fracture-related properties. These improvements in the mechanical properties of boron-modified Ti alloys are attributed to the TiB whiskers that precipitate in situ during processing. Boron-modified titanium alloys can be prepared using a variety of techniques, including conventional ingot metallurgy and powder metallurgy processes. These alloys can also be subjected to conventional thermomechanical processing operations such as forging, extrusion, and rolling to produce desired shapes with tailored microstructures. The wide range of compositions and processing methods available for Ti–B materials requires a thorough understanding of the relationships between the processing, microstructure, and properties, particularly how changes to one aspect will affect the others. The phase diagram of Ti–B alloys shows the eutectic reaction $liquid \rightarrow \beta^{Ti} + TiB$ [1]. In the hypereutectic Ti–B alloys, coarse primary TiB particles form above the eutectic temperature, followed by the formation of eutectic TiB whiskers below the eutectic temperature. In an earlier contribution, the presence of such coarse primary TiB particles has been shown in compacted as well as compacted plus extruded Ti–6Al–4V–1.7B alloys via reconstruction of their three-dimensional microstructures [2]. The presence of coarse primary TiB particles has an adverse effect on the fracture-sensitive mechanical properties of boron-modified Ti alloys, and as a result are

* Corresponding author. Tel.: +1 404 894 2887.
E-mail address: arun.gokhale@mse.gatech.edu (A.M. Gokhale).

1044-5803/$ - see front matter © 2006 Elsevier B.V. All rights reserved.
doi:10.1016/j.matchar.2006.07.015

Please cite this article as: S.I. Lieberman et al., Reconstruction of three-dimensional microstructures of TiB whiskers in powder processed Ti–6Al–4V–1B alloys, Materials Characterization (2006), doi:10.1016/j.matchar.2006.07.015.

not suitable for fracture critical applications (e.g., aerospace) [3]. Hypoeutectic Ti–B alloys, on the other hand, possess a good balance of mechanical properties [4]. Therefore, it is of interest to characterize microstructures of hypoeutectic Ti–B alloys and correlate them to the processing parameters and mechanical properties. Information from two-dimensional (2D) microstructural characterization would be inadequate for this purpose due to the complexity of the microstructures in these materials. Consequently, 3D representation and quantification of the microstructure would also be useful for the characterization, modeling, and simulation of these processing–microstructure–property relationships in hypoeutectic boron-modified Ti-alloys. In this contribution, we report reconstruction and visualization of 3D microstructures of a hypoeutectic alloy, Ti–6Al–4V–1B, in two different forms, compacted and compacted plus extruded. The 3D microstructures are reconstructed from stacks of large-area high-resolution montage serial sections. The next section gives a brief background on montage serial sectioning and 3D microstructure reconstruction and visualization, followed by the experimental work and results.

2. Montage serial sectioning and 3D microstructure reconstruction and visualization

A 3D microstructure can be rendered using techniques such as X-ray computed tomography (XCT), magnetic resonance imaging (MRI), and serial sectioning. Suitability of the specific reconstruction technique depends on the composition, processing, and microstructural length scales of the 3D microstructure of interest. Montage serial sectioning using optical microscopy is particularly suitable for microstructures where the features of interest have length scales ranging from 1 to 1000 μm and the reconstruction of a large volume of 3D microstructure at high resolution is desirable for characterization of the spatial arrangement and anisotropy of the microstructure. Such large 3D microstructural volume segments are also suitable to be incorporated into finite element-based simulations to predict the mechanical response of the material. The classical serial sectioning technique, which enables the reconstruction of a small volume segment of 3D microstructure, was developed in the 1970s [5]. This technique has been used in numerous investigations to study 3D microstructures of opaque materials [6–10]. An efficient montage-based serial sectioning technique is also available that permits the generation of a significantly large volume (relative to the length scale of the features of interest—in this study, the volume is on the order of cubic millimeters in size while the TiB whiskers are on the order of cubic micrometers) of 3D microstructure at a high resolution (~1 μm) [11–18]. To generate a large volume of 3D microstructure at high resolution, one may first reconstruct a small microstructural volume such as the one in Fig. 1a and then reconstruct many contiguous small volumes surrounding it, match their boundaries within the pixel resolution of the images, and paste them together to generate a large microstructural volume, as shown in Fig. 1b. For approximately the same metallographic effort, montage-based serial sectioning yields a microstructural volume containing a large number of features (such as whiskers, grains, or particles), which can provide a sufficiently large statistical sample for the study of topological aspects of microstructure such as feature connectivity. Recently, montage serial sectioning has also been implemented in a completely automated serial sectioning set-up that utilizes a robotic arm to move the specimen back and forth between the metallographic equipment (polishing, etching, etc.) and an optical microscope to generate the montage serial sections [17]. In this contribution, a montage serial sectioning technique is applied for the reconstruction and visualization of the TiB phase in a Ti–6Al–4V–1B alloy subjected to two different processing routes. Visualizations of the 3D microstructures are used to observe the effects of processing parameters on the morphology, anisotropy, and spatial distribution of the TiB phase.

3. Experimental

3.1. Materials, processing, and metallography

In this study, Ti–6Al–4V–1B produced via a pre-alloyed powder metallurgy approach at Crucible Research Corporation, Pittsburgh, PA, is investigated. In this

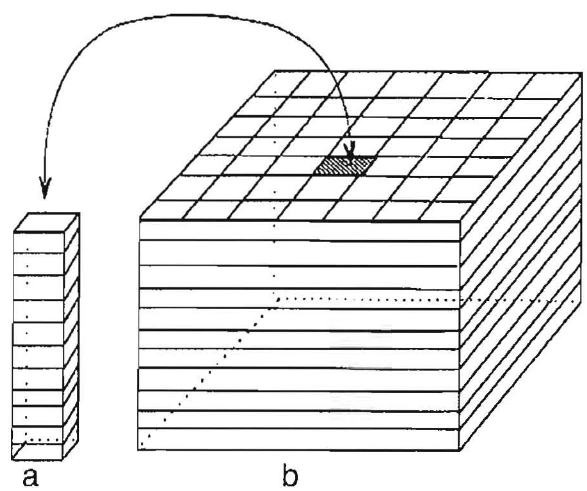

Fig. 1. (a) Small microstructural volume element constructed from a stack consisting of one field of view in each serial section. (b) Large volume of microstructure obtained from contiguous small volumes such as those in (a) by using montage serial sectioning [23].

Please cite this article as: S.I. Lieberman et al., Reconstruction of three-dimensional microstructures of TiB whiskers in powder processed Ti–6Al–4V–1B alloys, Materials Characterization (2006), doi:10.1016/j.matchar.2006.07.015.

process, the liquid melt of Ti–6Al–4V containing boron was rapidly solidified using inert gas atomization to produce Ti–6Al–4V–1B powder. The Ti–6Al–4V–1B powder of −100 mesh size (average particle size of 50 μm), was packed inside a thick-walled can of Ti–6Al–4V, vacuum outgassed at 300 °C for 24 h, and sealed. The can was heated to 1200 °C, soaked for 1 h, and then blind-die compacted in an extrusion chamber heated to 260 °C. The billet height was reduced by about 30% at a ram speed of 6.35 mm s^{-1}, and the compact was held at a pressure of 1400 MPa for 180 s and subsequently air-cooled to room temperature. A second billet blind die compacted by the same method was subsequently hot extruded at 1100 °C with an extrusion ratio of 16.5:1, at a ram speed of 6.35 mm s^{-1}, and air-cooled to room temperature. More information on the processing and 2D characterization of these alloys can be found in Ref. [3]. Specimens were sectioned from the compacted billet and extruded rod, and were prepared for metallographic observations using standard grinding and polishing techniques to obtain a final surface finish of 0.05 μm.

3.2. Metallographic serial sectioning

First, a “montage” of a large number of contiguous microstructural fields (225 fields in the present case) is constructed where each microstructural field of view is acquired at a high magnification (800× for the present microstructure). The basic principle for large-area high-resolution montage construction is described in detail by Louis et al. [12,19,20]. In the present work, the montages were created using the automated AxioVision digital image analysis system from Carl Zeiss, Inc., that utilizes the image cross-correlation function-based technique for matching the borders between contiguous microstructural fields. In the present case, each montage is a microstructural image of a large area (~1.76 mm^2) having a high resolution (~0.5 μm). Fig. 2a shows one such montage of 195 fields of view (FOV) which has been compressed for display, and Fig. 2b depicts a magnified view of the outlined region of the montage in Fig. 2a. Each region of the montage (Fig. 2a) has the high resolution of the image shown in Fig. 2c. Once the montage of the first serial section is created and stored in the computer memory, a small thickness of the specimen is removed by polishing (approximately 1 μm in the present case), and then a second montage is created at the region exactly below that in the first metallographic plane. In the present study, this polish–montage–polish procedure was repeated to obtain a stack of 75 montage serial sections.

Microhardness indents were used to locate the exact region of interest in successive serial sections and also to precisely measure the distance between consecutive serial sections [11,13]. An important practical problem in the reconstruction of a 3D microstructure from serial sections is that the successive serial sections may not be precisely aligned due to small translational and rotational displacements with respect to each other. In the present study, due to slight sample adjustment on the microscope stage, the montages of consecutive serial sections could become displaced by approximately ±10 pixels and ±5°, and therefore, it was essential to precisely align successive

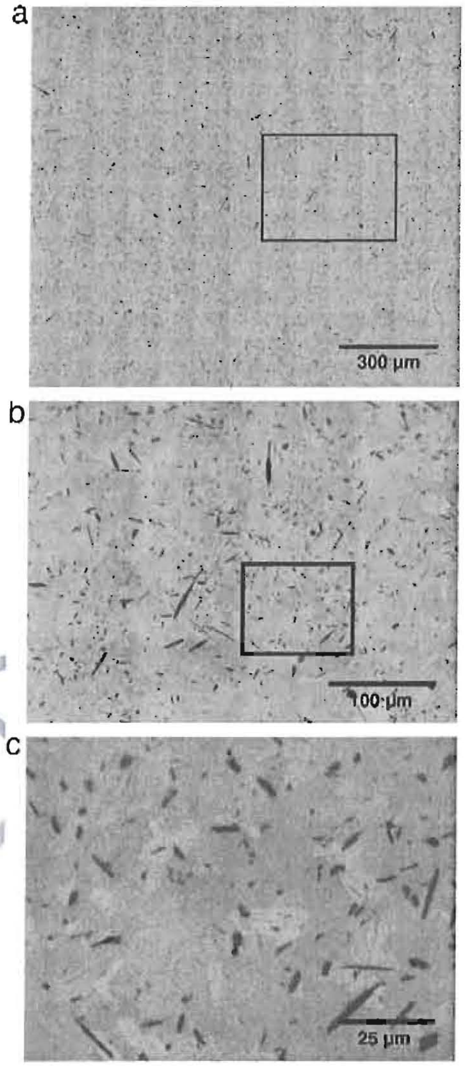

Fig. 2. Microstructure of *compacted* Ti–6Al–4V–1B alloy showing randomly oriented TiB whiskers: (a) montage of 195 fields of view covering an area of 1.76 mm^2 created by matching contiguous microstructural fields captured at a resolution of approximately 0.5 μm. The montage is digitally compressed for presentation. (b) Magnified view of the outlined region in (a). (c) One field of view (outlined region in (b)) of the montage. All of the 195 microstructural fields of the montage in (a) have the resolution of image (c).

Please cite this article as: S.I. Lieberman et al., Reconstruction of three-dimensional microstructures of TiB whiskers in powder processed Ti–6Al–4V–1B alloys, Materials Characterization (2006), doi:10.1016/j.matchar.2006.07.015.

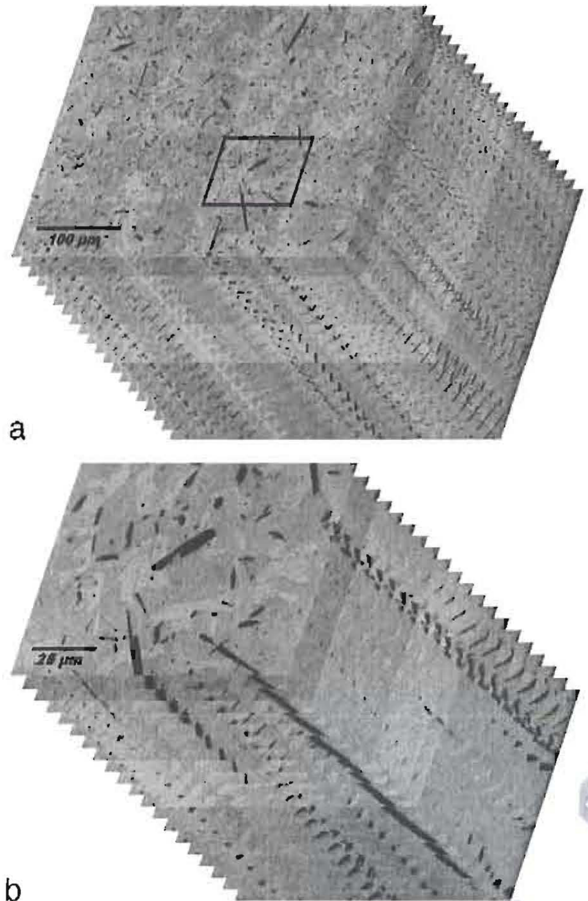

Fig. 3. (a) Stack of 20 montage serial sections for the *compacted* Ti–6Al–4V–1B microstructure. Each serial section in this figure contains 16 contiguous microstructural fields. (b) The magnified view of the outlined region of the stack of 20 montage serial sections in (a). This is the resolution of the individual microstructural fields.

serial sections. Alignment can be achieved by locating two common points (the microhardness indents were used for this purpose), in two consecutive serial sections and translating one image until the first common point is aligned in the two images. Then the image is rotated about this point until the second common point is also aligned. In the present case, this was accomplished by using the image analysis software KS 400 from Carl Zeiss, Inc., in which the images of the montage were digitally translated and rotated until they were aligned within ±1 pixel to the respective previous sections.

3.3. Reconstruction and visualization of three-dimensional microstructure

The stack of aligned serial sections essentially constitutes a volume image data set similar to those encountered in XCT and MRI. Therefore, the same three-dimensional microstructure visualization techniques are applicable. The 3D microstructure visualization can be achieved either by surface rendering or by volume rendering. Surface rendering involves the rendering of the iso-surface of the region of interest (ROI) from the volume data, whereas volume rendering is the rendering of *all* volume data by specifying opacity and color of each voxel (3D pixel). Volume rendered images can be incorporated into finite element-based computations [21]. Surface rendering leads to a reduction in the size of the data set because only the surface data are retained and requires the fitting of a surface in the volume data. Numerous algorithms are available for surface rendering, including the contour connecting algorithm [22] and the marching cube algorithm [23]. In the present work, the marching cube algorithm was employed for the surface rendering of the

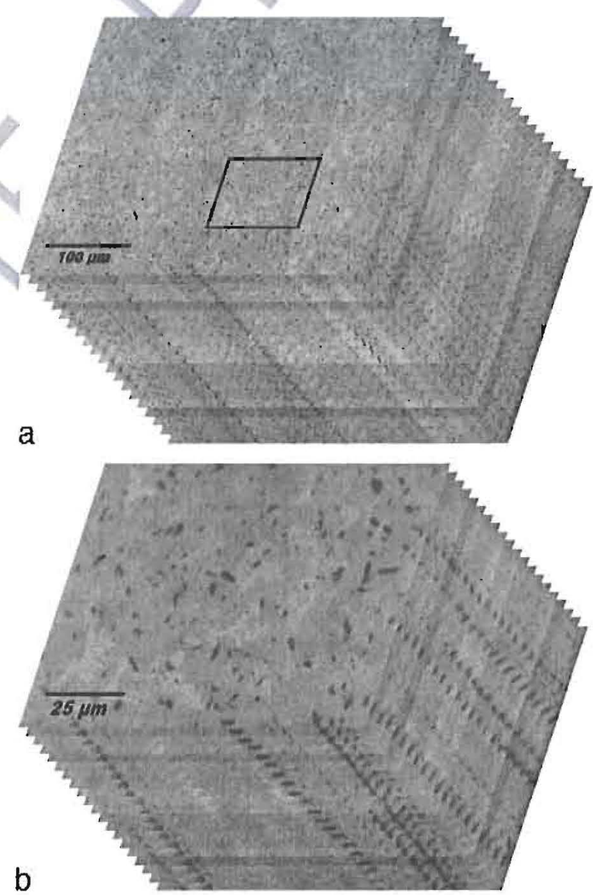

Fig. 4. (a) Stack of 20 montage serial sections for the *compacted plus extruded* Ti–6Al–4V–1B microstructure. The extrusion axis is perpendicular to the serial sections. Each serial section in this figure contains 16 contiguous microstructural fields. (b) The magnified view of the outlined region of the stack of 20 montage serial sections in (a). This is the resolution of the individual microstructural fields.

Please cite this article as: S.I. Lieberman et al., Reconstruction of three-dimensional microstructures of TiB whiskers in powder processed Ti–6Al–4V–1B alloys, Materials Characterization (2006), doi:10.1016/j.matchar.2006.07.015.

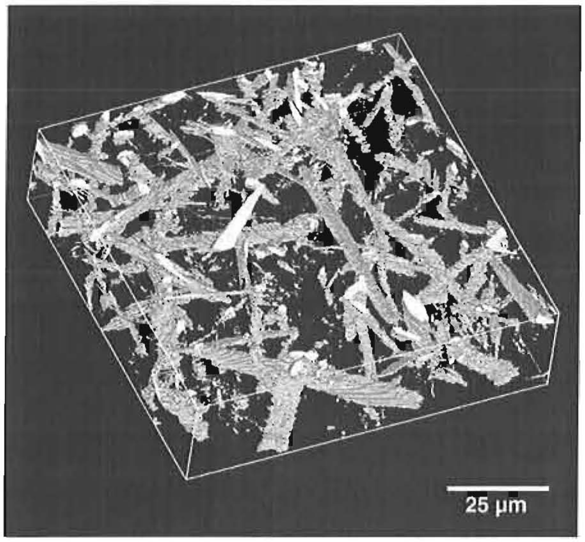

Fig. 5. Small segment of surface rendered 3D microstructure of *compacted* Ti–6Al–4V–1B. The TiB whiskers have isotropic uniform random orientations in this microstructure. The whisker size distribution is unimodal without any coarse primary TiB particles.

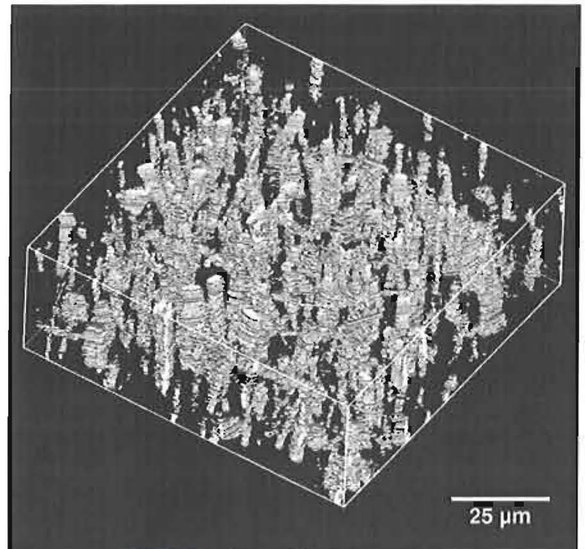

Fig. 6. Small segment of surface rendered 3D microstructure of *compacted plus extruded* Ti–6Al–4V–1B. The TiB whiskers of unimodal distribution have anisotropic orientations with the majority of the whiskers aligned parallel to the extrusion direction, which is the direction perpendicular to the serial sections.

3D microstructures, using the image analysis software VayTek VoxBlast 3.10.

4. Results and discussion

In the present work, the 3D microstructure visualization has been completed using 75 montage serial sections, with each montage serial section containing 225 contiguous microstructural fields grabbed at a magnification of 800× (with a pixel resolution of ~0.5 µm). Therefore, the resulting 3D data sets are useful for the characterization and visualization of the microstructure at fine as well as coarse length scales. Fig. 3 shows a stack of 20 aligned montage serial sections of the microstructure of compacted Ti–6Al–4V–1B having isotropic, uniform random eutectic TiB whiskers of unimodal length scale. Fig. 4 shows a stack of the compacted plus extruded microstructure having anisotropic morphological orientations of TiB. In this figure, the extrusion direction is perpendicular to the serial sections. The TiB whiskers aligned along the extrusion direction appear to have random orientation in the serial section 2D planes. Figs. 3a and 4a show 16 contiguous fields of view cropped from serial sections of 225 contiguous microstructural fields (these figures have been digitally compressed for presentation). Figs. 3b and 4b are the magnified views of the outlined regions in Figs. 3a and 4a, respectively, where each section is exactly the stack of serial sections generated by the single field of view type classical serial sectioning technique [5–10]. This is the magnification at which all microstructural fields of the montages have been grabbed. In Figs. 3b and 4b, changes in the sizes of the whiskers as well as the appearance and disappearance of features in successive serial sections can be observed.

Fig. 5 shows a volume segment of the surface-rendered 3D microstructure of the compacted alloy. In this condition, the TiB whiskers have uniform random morphological orientations in the 3D microstructure of a single length scale. Fig. 6 shows a segment of the surface-rendered 3D microstructure of the compacted plus extruded alloy depicting the spatial distribution of the anisotropic eutectic TiB whiskers. In this reconstructed 3D microstructure

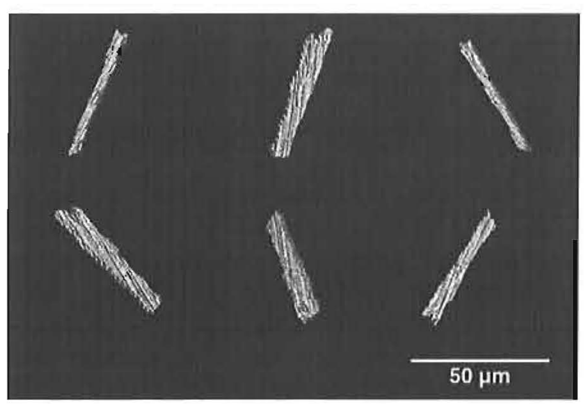

Fig. 7. Various views of a TiB whisker extracted from the 3D microstructure of *compacted* Ti–6Al–4V–1B.

Please cite this article as: S.I. Lieberman et al., Reconstruction of three-dimensional microstructures of TiB whiskers in powder processed Ti–6Al–4V–1B alloys, Materials Characterization (2006), doi:10.1016/j.matchar.2006.07.015.

segment, the majority of the TiB whiskers are aligned along the extrusion direction (which is normal to the top and bottom faces of the segment), although in the individual 2D sections perpendicular to the extrusion direction (Fig. 4), they appear to have random orientations due to non-circular cross-sections. Further, this 3D microstructure also reveals unimodal distribution of the eutectic TiB whiskers. In the surface-rendered images shown in Figs. 5 and 6, the images were digitally thresholded to completely remove the matrix and reveal only TiB. Note that these volume segments are only about 0.5% of the total microstructure volume collected from the stack of 75 montage serial sections (to produce the 3D rendering at the resolution of the TiB whiskers). Fig. 6 clearly shows that the eutectic TiB whiskers have anisotropic orientations after extrusion, and that the majority are aligned along the extrusion direction, which is the *z*-axis of the segment. Therefore, it can be concluded that plastic deformation during the extrusion process gives rise to rigid body rotations of the TiB whiskers, which confirms the conclusion reached by Schuh and Dunand on the basis of 2D microstructural observations [24]. Although the morphological orientation distribution of the eutectic TiB whiskers is different in the compacted microstructure as compared to the extruded microstructure, the spatial arrangement of the eutectic TiB whiskers appears to be uniformly random in both the 3D microstructures. Therefore, although the extrusion process leads to TiB whisker rotations, it does not give rise to spatial clustering of the whiskers. Fig. 7 shows multiple views of a eutectic TiB whisker extracted from the volume segment of the surface-rendered 3D microstructure of the compacted Ti–6Al–4V–1B microstructure in Fig. 5. Note that the surface "roughness" of the whisker is an artifact of the rendering software; from observations of the 2D sections, the TiB whiskers surfaces are smooth. The 3D morphology of the TiB whisker is clearly revealed in this reconstruction and is consistent among whiskers in both the compacted and compacted plus extruded microstructures.

5. Summary and conclusions

A montage serial sectioning technique has been used to generate high-resolution (~ 0.5 μm), large-volume (0.19 mm^3), 3D microstructures of a powder metallurgy Ti–6Al–4V–1B alloy containing TiB whiskers in two different process conditions (compacted and compacted plus extruded). The visualization of the reconstructed 3D microstructure provided important insights on the 3D morphologies and distribution of the TiB phase. The alloy contains a single length-scale eutectic TiB phase. In the compacted condition, the TiB whiskers have uniform random angular orientations, whereas after extrusion, they are aligned along the extrusion direction. In both conditions, the spatial arrangement of TiB is uniform random without clustering.

Acknowledgements

This research is supported through research grants from the Air Force Office of Scientific Research (AFOSR Grant Number F49620-01-1-0045). Dr. J. S. Tiley is the AFOSR Program Manager for this grant. The financial support is gratefully acknowledged. The authors also acknowledge helpful discussions with Dr. D.B. Miracle of the Air Force Research Laboratory. Any opinions, findings, and conclusions or recommendations expressed in this contribution are those of the authors and do not necessarily reflect the views of the funding agencies.

References

[1] Murray JL, Liao PK, Spear KE. In: Baker H, editor. Binary alloy phase diagrams. Materials Park, OH: ASM International; 1992. p. 285.
[2] Lieberman SI, Gokhale AM, Tamirisakandala S. Scr Mater 2006;55:63–8.
[3] Tamirisakandala S, et al. Scr Mater 2005;53:217.
[4] Boehlert C. et al. Scripta Materialia, in press.
[5] Rhines FN, Craig KR. Metall Trans, A, Phys Metall Mater Sci 1976;7A:1729.
[6] Sidhu RS, Chawla N. Mater Charact 2004;52:225.
[7] Li M, Ghosh S, Richmond O, Weiland H, Rouns TN. Mater Sci Eng A Struct Mater: Prop Microstruct Process 1999;265:153.
[8] Wu KM, Enomoto M. Scr Mater 2002;46:569.
[9] Kral MV, Mangan MA, Spanos G, Rosenberg RO. Mater Charact 2000;45:17.
[10] Yokomizo T, Enomoto M, Spanos G, Rosenberg RO. Mater Sci Eng A Struct Mater: Prop Microstruct Process 2003;344A:261.
[11] Tewari A, Gokhale AM, German RM. Acta Mater 1999;47:3721.
[12] Gokhale AM, Tewari A. J Microsc 2000;200:277.
[13] Tewari A, Gokhale AM. Mater Charact 2001;46:329.
[14] Dighe MD, Tewari A, Patel GR, Mirabelli T, Gokhale AM. Trans Am Foundry Soc 2000;99:353.
[15] Lee SG, Gokhale AM, and Sreeranganathan A. Materials Science and Enineering, in press.
[16] Singh H, Gokhale AM. Mater Charact 2005;54:21.
[17] Spowart JE, Mullens HM, Puchala BT. J Met 2003:35.
[18] Lee SG, Gokhale AM, and Milhans JL Trans. American Foundry Society, in press.
[19] Louis P, Gokhale AM. Metall Mater Trans A Phys Metall Mater Sci 1995;26A:1449.
[20] Louis P, Gokhale AM. Acta Mater 1996;44:1519.
[21] Sabella P. Comput Graph 1988;22:51.
[22] Keppel E. IBM J Res Develop 1975;19:2.
[23] Lorensen EW, Cline HE. Comput Graph 1987;22:38.
[24] Schuh C, Dunand DC. Int J Plast 2001;17:317.

Please cite this article as: S.I. Lieberman et al., Reconstruction of three-dimensional microstructures of TiB whiskers in powder processed Ti–6Al–4V–1B alloys, Materials Characterization (2006), doi:10.1016/j.matchar.2006.07.015.

Attachment 2

US Patent Application

Title:

Method of Producing High Strength, High Stiffness and High Ductility Titanium Alloys

Co-inventors:

D.B. Miracle, S. Tamirisakandala, R.B. Bhat, D.J. McEldowney, W.M. Hanusiak, R. Grabow, J. Fields, C.F. Yolton, E. Bono

Patent application filed with USPTO in June 2006

TITLE OF THE INVENTION

METHOD OF PRODUCING HIGH STRENGTH, HIGH STIFFNESS AND HIGH DUCTILITY TITANIUM ALLOYS

CROSS-REFERENCES TO RELATED APPLICATIONS

[0001] N/A

STATEMENT REGARDING FEDERALLY SPONSORED RESEARCH OR DEVELOPMENT

[0002] The present invention may be manufactured and used by or for the Government of the United States for all governmental purposes without the payment of any royalty.

REFERENCE TO A MICROFICHE APPENDIX

[0003] N/A

BACKGROUND OF THE INVENTION

1. Field Of The Invention

[0004] The present invention relates generally to methods for enhancing the performance of conventional titanium alloys without a reduction in damage tolerance and, more specifically, to a method for producing homogeneous microstructure in the broad family of titanium alloys including, but not limited to Ti-6wt.%Al-4wt.%V, Ti-5Al-2.5Sn, Ti-6A1-2Sn-4Zr-2Mo-O.lSi.

2. Description Of The Background Art

[0005] Titanium alloys offer attractive physical and mechanical property combinations that make them suitable for a variety of structural applications in various industries (e.g. aerospace) to obtain significant weight savings and reduced maintenance costs compared to other metallic materials such as steels. There have been several efforts to further increase the strength and stiffness of conventional titanium alloys to obtain enhanced performance. These approaches involve addition of particulates, short fibers, or continuous fibers that possess high strength and stiffness. Although these prior art approaches increase the strength and stiffness of conventional titanium alloys significantly, the increases are obtained with an accompanying drastic reduction in ductility and damage tolerance owing to the presence of brittle reinforcement, which restricts their usage in fracture-sensitive applications. A value of 5% tensile elongation is often considered in structural applications to separate ductile from brittle behavior.

[0006] Accordingly, a purpose of the present invention is to provide a novel methodology for producing titanium alloys with significant enhancement in strength and stiffness relative to conventional titanium alloys while maintaining adequate ductility. The method described herein involves addition of a small amount of boron below a critical level, and deforming the alloy at a specified range of temperature and deformation rate, to obtain uniform microstructure.

BRIEF SUMMARY OF THE INVENTION

[0007] In accordance with the new and improved method of the present invention, the strength and stiffness of titanium alloys are increased, while maintaining ductility, by the addition of boron and controlled processing to obtain uniform microstructure.

[0008] Important features of the present method are as follows:

1. The boron concentration in the titanium alloy should be at or below the eutectic limit so that it does not possess any coarse primary TiB particles;

2. The titanium alloys containing boron are heated above the beta transus temperature (temperature at which the titanium alloy transforms fully to high temperature body-centered cubic beta phase) to completely force out any supersaturated boron (boron trapped inside the lattice of titanium under non-equilibrium solidification conditions); and

3. The boron-modified titanium alloy is subjected to deformation at a slow rate, e.g., extrusion at slow speed, to avoid damage to the TiB micro-constituent which reduces ductility.

BRIEF DESCRIPTION OF THE DRAWINGS

[0009] FIG. 1 is a binary titanium-boron phase diagram;

[0010] FIG. 2(a) is an electron micrograph of coarse primary TiB particles in a titanium alloy composition (Ti-6Al-4V-l.7B) above the eutectic limit;

[0011] FIG. 2(b) is a fractograph of a tensile specimen showing preferential crack initiation at coarse primary TiB particles;

[0012] FIG. 3(a) is a graph of ductility versus temperature in as-compacted Ti-6Al-4V-1B alloy with different carbon concentrations;

[0013] FIG. 3(b) is a graph of ductility versus temperature in an extruded Ti-6Al-4V-1B alloy with different carbon concentrations;

[0014] FIG. 4(a) is a backscattered electron micrograph of a Ti-6Al-4V-1B alloy compacted at 1750°F (below the beta transus);

[0015] FIG. 4(b) is a backscattered electron micrograph of a Ti-6Al-4V-1B alloy compacted at 1980°F (above the beta transus);

[0016] FIG. 5(a)) is a backscattered electron micrograph of a Ti-6Al-4V-1B-0.1C alloy extruded at a ram speed of 100 inch/min., taken along the extrusion direction;

[0017] FIG. 5(b) is a backscattered electron micrograph of a Ti-6Al-4V-1B-0.1C alloy extruded at a ram speed of 100 inch/min., taken along the transverse direction;

[0018] FIG. 5(c) is a backscattered electron micrograph of a Ti-6Al-4V-1B-0.1C alloy extruded at a ram speed of 15 inch/min., taken along the extrusion direction;

[0019] FIG. 5(d) is a backscattered electron micrograph of a Ti-6Al-4V-1B-0.1C alloy extruded at a ram speed of 15 inch/min., taken along the transverse direction; and

[0020] FIG. 6 is a graph showing the tensile properties of a slow speed extruded Ti-6Al-4V-1B alloy as compared with a typical Ti-6Al-4V alloy

[0021]

DETAILED DESCRIPTION OF THE INVENTION

[0022] The present invention provides a novel method of increasing the strength and stiffness while maintaining the ductility of titanium alloys by the addition of boron and controlled processing. This new and improved method causes the natural evolution of fine and uniform microstructural features. Although the description hereinafter is specific to a powder metallurgy processing technique, the invention is equally applicable to other powder processing techniques.

[0023] In the pre-alloyed powder metallurgy approach, the boron is added to the molten titanium alloy and the melt is atomized to obtain boron-containing titanium alloy powder. The powder may be consolidated and/or formed via

conventional techniques such as hot isostatic pressing, forging, extrusion, and rolling.

[0024] The method of the present invention includes four important elements which are described hereinafter.

1) <u>Boron Level At or Below the Eutectic Limit</u>

[0025] While boron is fully soluble in liquid titanium, its solubility in the solid phase is negligible. The binary Titanium-Boron phase diagram shown in Fig. 1 illustrates that there exists an eutectic reaction at a temperature of 2804^0F (1 540^0C) and boron concentration of 2 wt.%. Similar eutectic reactions are expected in other titanium alloys modified with boron with a change in the eutectic temperature and boron concentration. When alloys with compositions that contain boron concentrations above the eutectic limit are solidified, very coarse primary TiB particles grow in the two phase (liquid plus TiB) region and are retained in the fully solidified microstructure. Although these particles provide significant strength and stiffness improvements, drastic reduction in ductility occurs. An example of the effect of the coarse primary TiB particles is illustrated in Fig. 2 for a Ti-6A1-4V-1.7B (all concentrations expressed in weight percent) alloy which is above the eutectic composition for this titanium alloy. The presence of coarse TiB particles larger than 200 μm is seen in Fig. 2(a) and the preferential initiation of fracture at these particles in a tensile specimen causing premature failure (ductility of ~3%) is recorded in Fig. 2(b). Therefore, the present invention is applicable to any conventional titanium alloy that contains boron concentration below the eutectic limit and that does not possess any of the coarse primary TiB particles.

2) <u>Carbon Level Below a Critical Limit</u>

[0026] It has been discovered that the carbon concentration also significantly influences the ductility of boron-modified titanium alloys and it is important to keep the carbon level below a critical limit to avoid an unacceptable loss of ductility. Unlike boron, the solid solubility of carbon in titanium is high (up to 0.5 weight %) and carbon in titanium could cause embrittlement. The carbon concentration, therefore should be contolled depending on the alloy composition and processing parameters to achieve acceptable ductility values. For example, Fig. 3 shows results from a study of a Ti-6A1-4V-1B alloy with varying carbon concentrations from 0.05 to 0.35% in as-compacted (Fig. 3a) and extruded (Fig. 3b) conditions. For the selected process conditions, these variations illustrate that the ductility significantly drops to below 4% for carbon concentrations above 0.1%.

3) <u>Thermal Exposure Above the Beta Transus</u>

[0027] Owing to negligible solid solubility of boron in titanium, excess boron is trapped (supersaturated) inside the lattice of titanium under non-equilibrium solidification conditions (e.g. powder manufacture via rapid solidification techniques such as gas atomization). Titanium alloy with supersaturated boron is inherently brittle and possesses low ductility values. It has been discovered that the supersaturated boron can be forced out via thermal exposure at a high temperature. Experiments to determine the optimum temperature for eliminating the supersaturation are illustrated in Fig. 3. From these experiments, it is concluded that the material should be exposed above the beta transus temperature (temperature at which the titanium alloy transforms fully to high temperature body-centered cubic beta phase) to completely force out the supersaturated boron. Thermal exposure also influences microstructural parameters such as size, distribution, and inter-particle spacing of TiB particles,

and grain size and morphology of the titanium phases. These microstructural parameters significantly influence the mechanical properties.

[0028] Thermal exposure at lower temperatures results in close inter-particle spacing which restricts the ductility. Exposure above the beta transus increases the inter-particle spacing which improves the ductility. The rate at which the material is cooled after thermal exposure alters the grain size and morphology, both of which also significantly influence the ductility. Controlled slow cooling from above the beta transus produces fine-grained equiaxed alpha-beta microstructure due to the influence of TiB particles on the phase transformation reaction of high temperature beta to room temperature alpha. The beta transus varies with the composition of principal alloying elements in conventional titanium alloys, and, e.g., is 1850 ± 50^{0}F for Ti-6A1-4V. Thermal exposure may be applied via hot isostatic pressing, extrusion, or another suitable consolidation method, or by thermal treatment before or after consolidation, or thermo-mechanical processing. The effects of thermal treatments in HIP compacts and extrusions are shown in Fig. 3. Microstructures of Ti-6A1-4V-1 B powder compacted below and above the beta transus are shown in Fig. 4, which clearly demonstrates the influence of thermal exposure temperature on the microstructural evolution.

4) <u>Deformation Rate Control to Avoid Microstructural Damage</u>

[0029] The rate at which boron-modified titanium alloy is subjected to deformation also has significant influence on the final microstructure and mechanical properties. Microstructures of Ti-6A1-4V-1 B-0.1 C material extruded at a fast ram speed (100 inch/mm) and slow speed (15 inch/mm) are shown in Fig. 5. The material extruded at high-speed (Figs. 5a and 5b) exhibited microstructural damage manifested as TiB particle fracture and cavitation at the ends of TiB, which reduce the ductility. The material extruded at slow-speed (Figs. 5c and 5d),

on the other hand, is completely free from microscopic damage. Although, the demonstrations are made using selected processes and deformation rates, the method of this invention is applicable to the full range of consolidation approaches and thermo-mechanical processes, and covers a broad range of safe deformation rates necessary to avoid damage to the TiB microconstituent.

[0030] The properties of slow-speed extruded Ti-64-1 B are compared with a typical Ti-6A1-4V alloy [2] in Fig. 6. An increase in stiffness (modulus) by ~25% and strength by ~35%, while maintaining equivalent ductility level (>10%), is obtained in boron-modified Ti alloy processed under controlled conditions described above.

[0031] It will be readily seen, therefore, that the new and improved method of the present invention increases the strength and stiffness of conventional titanium alloys without significant loss in ductility, thus significantly enhancing the structural performance of titanium alloys.

[0032] Boron-modified titanium alloys could be produced using traditional processing methods and conventional metalworking (e.g. forging, extrusion, rolling) equipment can be used to perform controlled processing. Therefore, the improved performance with the use of the present method is obtained without any increase in material or processing cost.

[0033] Titanium alloys with 25-35% increases in strength and stiffness could replace existing expensive components for high performance and could enable new structural design concepts for weight and cost reduction.

[0034] While the invention has been described in connection with what is presently considered to be the most practical and preferred embodiments, it is to be understood that the invention is not to be limited to the disclosed embodiments,

but on the contrary, is intended to cover various modifications and equivalent arrangements included within the spirit and scope of the appended claims.

CLAIMS

1. A method of producing a high strength, high stiffness and high ductility titanium alloy, comprising:

combining a titanium alloy with boron so that the boron concentration in the boron-modified titanium alloy does not exceed the eutectic limit,

maintaining the carbon concentration of the boron-modified titanium alloy below a specified limit to avoid embrittlement,

heating the boron-modified alloy to a temperature above the beta transus temperature to eliminate any supersaturated excess boron, and

deforming the boron-modified titanium alloy at a speed slow enough to prevent microstructural damage and reduced ductility.

2. The method of claim 1 wherein the boron is added to a molten titanium alloy and the melt is atomized to obtain boron-containing titanium alloy powder.

3. The method of claim 2 wherein the boron-containing titanium alloy powder is consolidated and/or formed by hot isostatic pressing, forging, extrusion or rolling.

4. The method of claim 2 wherein the boron is in liquid or powder form.

5. The method of claim 1 wherein the titanium alloy is selected from the group consisting of commonly used titanium alloys such as Ti-6Al-4V, Ti-5Al-2.5Sn and Ti-6Al-2Sn-4Zr-2Mo-0.1Si.

6. A method of producing a high strength, high stiffness and high ductility titanium alloy, comprising:

combining a titanium alloy with boron so that the boron concentration in the boron-modified titanium alloy does not exceed the eutectic limit when the titanium alloy and boron are heated to a predetermined temperature.

7. The method of claim 6 further comprising maintaining the carbon concentration of the boron-modified titanium alloy low enough to avoid embrittlement.

8. The method of claim 7 further comprising heating the boron modified alloy to a temperature above the beta transus temperature to eliminate any supersaturated excess boron.

9. The method of claim 6 further comprising heating the boron-modified alloy to a temperature above the beta transus temperature to eliminate any supersaturated excess boron.

10. The method of claim 6 further comprising deforming the boron-modified titanium alloy at a speed slow enough to prevent microstructural damage and reduced ductility.

11. The method of claim 9 further comprising deforming the boron-modified titanium alloy at a speed slow enough to prevent microstructural damage and reduced ductility.

ABSTRACT OF THE DISCLOSURE

A method of producing a high strength, high stiffness and high ductility titanium alloy, comprising combining the titanium alloy with boron so that the boron concentration in the boron-modified titanium alloy does not exceed the eutectic limit when the titanium alloy and boron are heated to a predetermined temperature. The carbon concentration of the boron-modified titanium alloy is maintained low enough to avoid embrittlement. The boron-modified alloy is heated to a temperature above the beta transus temperature to eliminate any unsaturated excess boron. The boron-modified titanium alloy is deformed at a speed slow enough to prevent microstructural damage and reduced ductility.

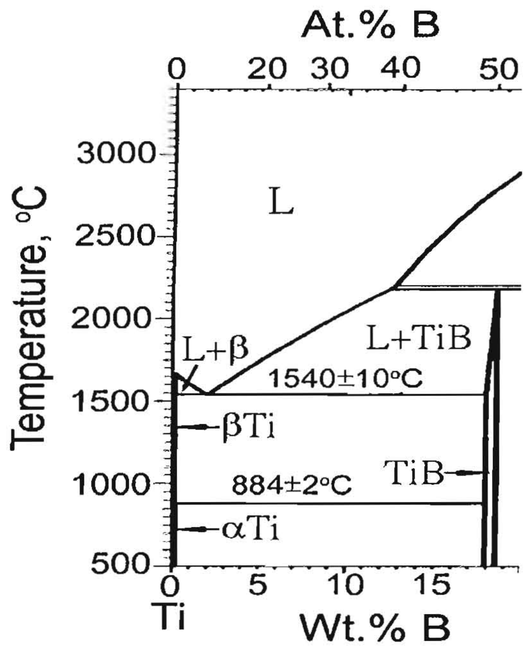

Fig. 1 Titanium rich section of the Ti-B binary phase diagram.

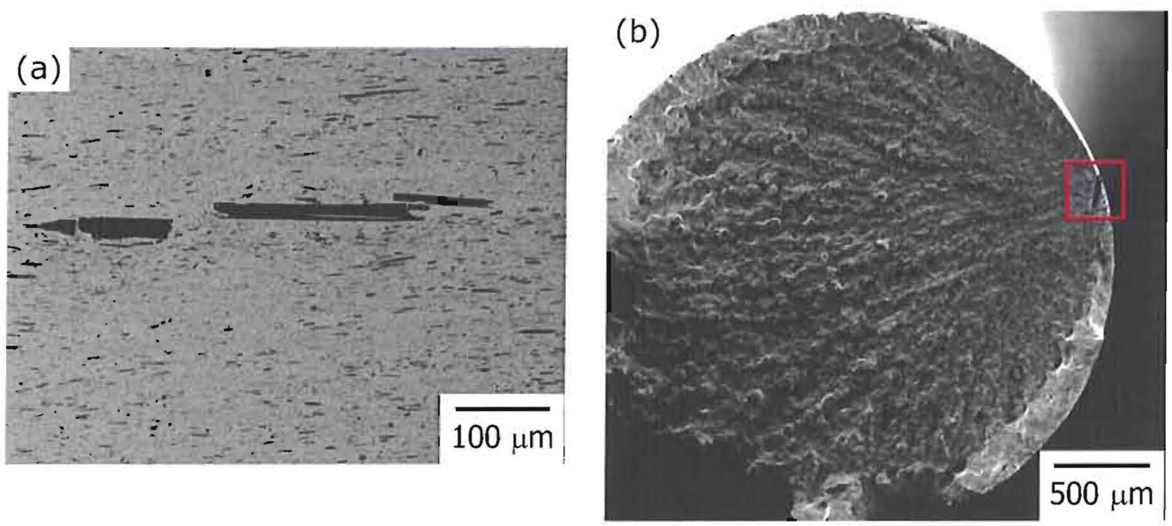

Fig. 2 (a) Coarse primary TiB particles in a titanium alloy composition above the eutectic limit (Ti-6Al-4V-1.7B) and (b) fractograph of a tensile specimen illustrating their influence on causing preferential crack initiation at these particles that leads to premature brittle failure.

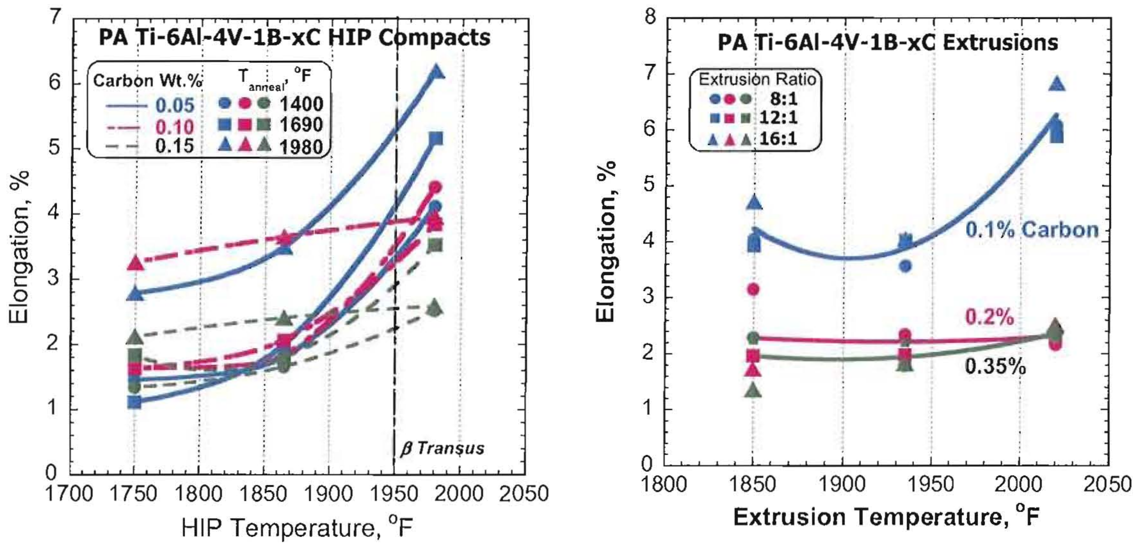

(a) (b)

Fig. 3 Effect of temperature and carbon content on the ductility of Ti-6Al-4V-1B alloys after a) HIP and (b) extrusion.

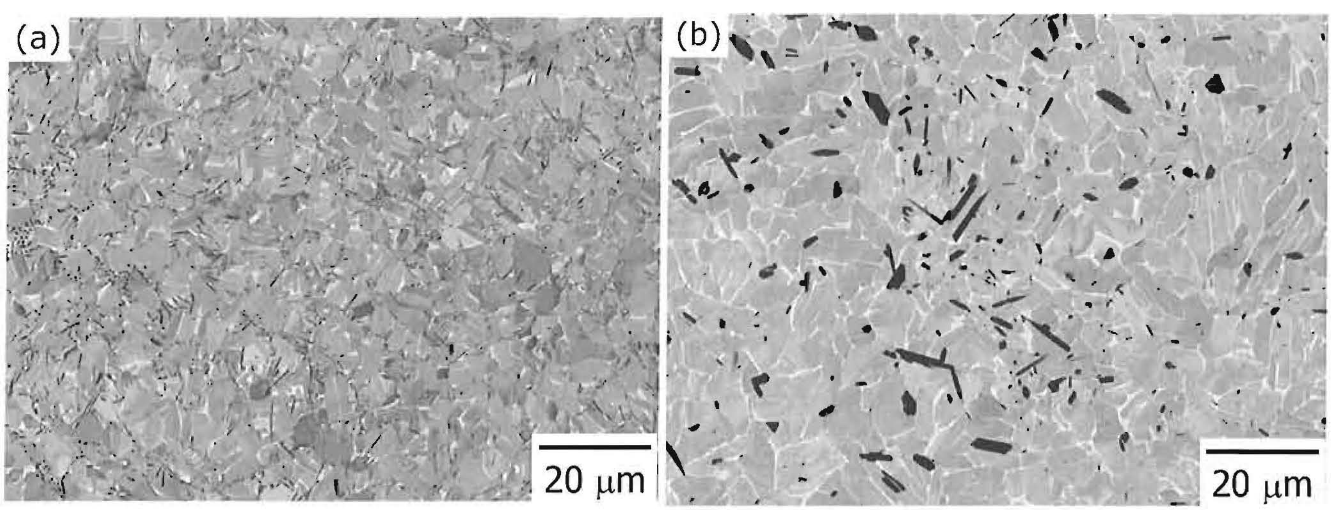

Fig. 4 Backscatterd electron micrographs of Ti-64-1B alloy HIPed at (a) 1750°F (below the beta transus) and (b) 1980°F (above the beta transus).

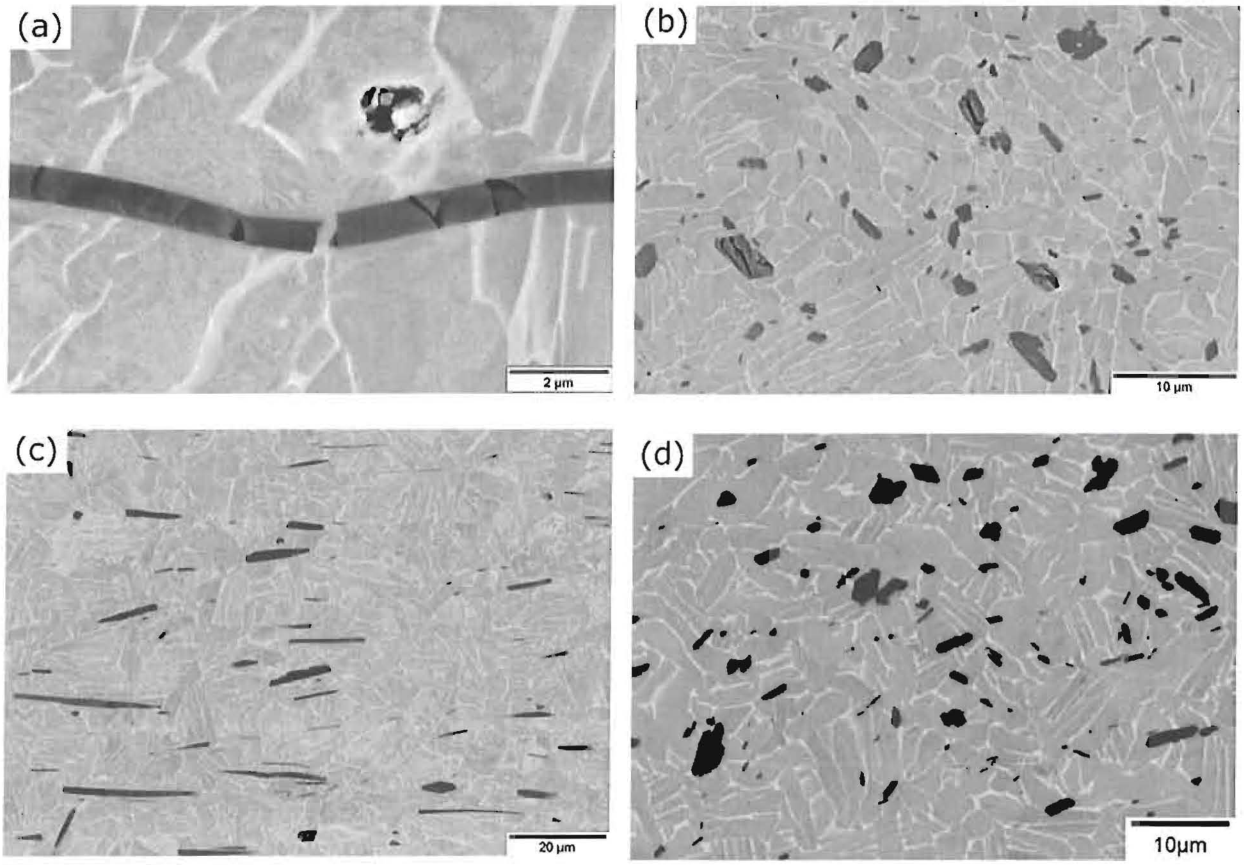

Fig. 5 Backscattered electron micrographs of Ti-64-1B-0.1C alloy extruded at a ram speed of (a, b) 100 inch/min and (c, d) 15 inch/min. (a, c) are along the extrusion direction and (b, d) are along the transverse direction.

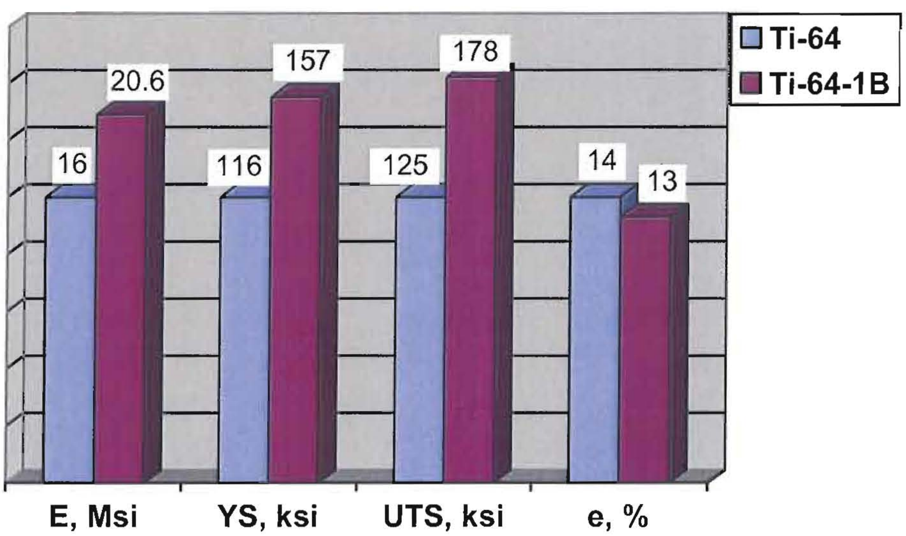

Fig. 6 Tensile properties of extruded Ti-64-1B alloy compared with Ti-64.